Real-time management of distributed multi-energy resources in multi-energy networks

António Coelho[1*], José Iria[2], Filipe Soares[1], João Peças Lopes[3]

[1] Centre for Power and Energy Systems, INESC TEC, 4200-465 Porto, Portugal

[2] College of Engineering & Computer Science, Australian National University, Canberra, Australia

[3] Faculty of Engineering of University of Porto (FEUP), Porto, Portugal

[*] Corresponding author: antonio.m.coelho@inesctec.pt

Please cite this paper as: A. Coelho, J. Iria, F. Soares, J.P. Lopes, Real-time management of distributed multi-energy resources in multi-energy networks, Sustainable Energy, Grids and Networks. 34 (2023) 101022. doi: 10.1016/j.segan.2023.101022.

Abstract

The replacement of fossil fuel power plants by variable renewable energy sources is reducing the flexibility of the energy system, which puts at risk its security. Exploiting the flexibility of distributed multi-energy resources through aggregators presents a solution for this problem. In this context, this paper presents a new hierarchical model predictive control framework to assist multi-energy aggregators in the network-secure delivery of multi-energy services traded in electricity, natural gas, green hydrogen, and carbon markets. This work builds upon and complements a previous work from the same authors related to bidding strategies for day-ahead markets – it closes the cycle of aggregators' participation in multi-energy markets, i.e., day-ahead bidding and real-time activation of flexibility services. This new model predictive control framework uses the alternating direction method of multipliers on a rolling horizon to negotiate the network-secure delivery of multi-energy services between aggregators and distribution system operators of electricity, gas, and heat networks. We used the new model predictive control framework to conduct two studies. In the first study, we found that considering multi-energy network constraints at both day-ahead and real-time optimization stages produces the most cost-effective and reliable solution to aggregators, outperforming state-of-the-art approaches in terms of cost and network security. In the second study, we found that the adoption of a green hydrogen policy by multi-energy aggregators can reduce their consumption of natural gas and respective CO_2 emissions significantly if carbon and green hydrogen prices are competitive.

Keywords: aggregators, distribution networks, energy markets, multi-energy systems, optimization.

Nomenclature

Indices and sets

$d \in \{E, G, H, H2\}$	Energy vectors
$a \in \{S, R\}$	Supply and return networks
$j \in J$	Clients
$J_n \subset J$	Clients at bus n
k	ADMM iteration
$m, n, i, j \in N^E, N^G, N^H$	Buses/nodes of electricity, gas, and heat networks

$(m,n),(i,j) \in B^E, B^G, B^H$	Lines/pipelines from bus m to bus n for electricity, gas, and heat networks
$N^{NG} \subset N^G$	Gas nodes with natural gas injection
$N^{GL} \subset N^G$	Gas nodes with natural gas loads
$N^{H2} \subset N^G$	Gas nodes with hydrogen resources
$s \in \{En, U, D\}$	Delivery scenarios per energy vector
$t, y \in T$	Time intervals
$v \in \{E, G, H2, H2O, O2, C\}$	Markets/products

Superscripts

Abs	Absolute
Amb	Ambient temperature of pipelines' surroundings
AGC	Automatic generation control
C	Carbon market
CFA	Free allowances of the carbon market
CHP	Combined heat and power
CO_2	Carbon dioxide
D	Downward reserve
DA	Day-ahead
DH	District heating
$Dual$	Dual residual
E	Electricity
EH	Heat pump
En	Energy
End	End of pipeline
F	Power flow
G	Gas
GL	Natural gas loads
GO	Guarantees of origin
H	Heat
HLG	Heat loads and generators
HV	Hydrogen vehicles
H_2	Hydrogen
H_2O	Water
IL	Inflexible load
In	Input flow
Mix	Gas mixture
Net	Network injection
NG	Natural gas injection
O	Outdoor temperature
Out	Output flow
$O2$	Oxygen
$Primal$	Primal residual
PV	Photovoltaic system
$P2G$	Power-to-gas (or electrolyzers)
R	Return temperature
RT	Real-time
S	Supply temperature
St	Standard conditions of temperature and pressure
$Start$	Start of pipeline
Sto	Battery energy storage system
U	Upward reserve

$+, -$	Charging, discharging of electric storage systems or positive, negative
$\overline{\ }, \underline{\ }$	Maximum, minimum
$\hat{\ }$	DSOs replicated values

Parameters

c	Conversion factors
CP	Water specific heat (J/kg.°C)
d	Diameter of pipeline (mm)
e	Efficiency factor
FA	Free allowances (tCO_2)
h	Heat transfer coefficient ($W/°C.m$)
k	Coefficient of pressure loss in water pipelines
K	Resistance pipeline coefficient
L	Length of pipeline (m)
LHV	Low heating value (kWh/kg)
r	Resistance of power lines (p.u.)
R	Resistance of thermal buildings (°C/kW)
SB	Base power (kVA)
x	Reactance of power lines (p.u.)
Δt	Length of the time interval t (h)
β	Thermal constant
η	Efficiency/coefficient of performance
γ	Hydrogen storage energy dissipation rate (%)
λ	Price (€/kWh, €/kW, €/tCO_2, €/L or €/kg)
μ	Parameter of response of CHPs
ϕ	Ratio of secondary reserve activation
ρ	Penalty of the augmented Lagrangian (€/kW^2)
τ	Residual
ϵ	Absolute tolerance
a	Dimension of the residuals
ϑ	Heat gains and losses not modeled explicitly (°C)

Variables

A	Allowances (tCO_2)
b	Binary variable
D	Downward band (kW)
HHV	Higher heating value (MJ/m^3)
ℓ	Square of the current magnitude (p.u.)
m	Mass flow of pipelines (kg/s)
mq	Mass flows of heat loads and generators (kg/s)
p	Pressure (gas: bar, heat: Pa)
P	Power (kW)
q	Gas flows (m^3/h)
Q	Reactive power (p.u.)
S	Specific gas gravity
SOC	State-of-charge (kWh)
U	Upward band (kW)
v	Square of the voltage magnitude (p.u.)
w	Hydrogen fraction
WI	Wobbe index (MJ/m^3)
X	Internal variables of the aggregator problem
Y	Internal variables of the energy DSO problem

φ	Auxiliary binary variable
π	Dual variables of the augmented Lagrangian (€/kW)
θ	Temperature (gas network: °K, other: °C)

1. Introduction

1.1. Motivation and Aim

With the Paris Agreement, countries worldwide have agreed on making efforts to keep the rising of global temperature below 2°C. To achieve this goal, the European Union defined its own goal to decrease CO_2 emissions by at least 55% by 2030 [1]. The decarbonization of the energy system is seen as the first step to achieving this goal. This can be done by replacing fossil-fuel power plants with renewable energy power plants, and at the same time reducing energy consumption through energy efficiency programs. To promote this transformation, the European Union implemented a carbon market to tax carbon-intensive technologies.

The decarbonization of the electricity, gas and heat systems is an important part of the whole decarbonization process. The electricity system started to be decarbonized several years ago through the integration of renewable energy sources, such as wind or PV (photovoltaic) farms. The natural gas systems, such as gas networks, are planning to be partially decarbonized through the injection of green hydrogen[1] and biogas. Green hydrogen can also be seen as a storage solution for the excess electricity produced by renewable energy sources, since it can be stored, and later converted into electricity through fuel cells. Moreover, the use of green hydrogen in transportation is also gaining traction which will likely increase the number of hydrogen resources connected to the electricity network. Lastly, heating systems powered by fossil fuels are planned to be replaced by high-efficiency electric heating systems, such as heat pumps. Although, high-efficiency combined heat and power (CHP) systems may also play an important role in the transition period.

The deployment of these low-carbon emission technologies has contributed to the reduction of CO_2 emissions. However, some of these technologies, such as renewable energy resources, have been causing some problems in the energy system, due to their variability nature. To counteract these problems, the flexibility of distributed multi-energy resources (DMERs)[2] must be used. In this context, aggregators provide a technological solution to transform the flexibility of DMERs into multi-energy market services, which can be used to compensate the variability of renewable energy resources. Nonetheless, this solution also brings new challenges for the operation of the energy system. One of the challenges is to ensure that the energy services traded by aggregators in multi-energy markets can be delivered without violating the constraints of multi-energy networks, and the privacy of any of the energy stakeholders involved. To address this challenge, this paper proposes a new hierarchical model predictive control (MPC) framework.

1.2. Literature review

Aggregators need decision-support optimization tools to transform the flexibility of DMERs into multi-energy services, which can be traded into multi-energy markets, such as electricity (energy and reserve), natural gas, green hydrogen, and carbon markets. In this context, aggregators rely on two groups of optimization algorithms: 1) bidding optimization algorithms to compute bids

[1] Green hydrogen is produced through electrolyzers with renewable energy, making it carbon-free.
[2] Distributed multi-energy resources include PVs, battery energy storage systems, CHPs, thermal loads, and hydrogen technologies.

for day-head markets; and 2) real-time optimization algorithms to ensure the reliable delivery of the bids in real-time.

The first group of optimization algorithms is rich in the literature. Several research papers propose bidding models to optimize DMERs, such as EVs [2][3][4][5][6], PVs [4][5][6], battery energy storage systems (BESSs) [7][8], thermal loads [4][5][6][7] or CHPs [7][8] for day-ahead market participation. The bidding models can be deterministic [2][3], stochastic [4][5][6] or even robust [9] optimization models. They can compute network-secure or network-free bids for day-ahead electricity [3][4][5][6], natural gas [7][8], and carbon [7] markets. The network-free bids are computed by bidding models [2][3][4][5][6][8] that do not consider the constraints of multi-energy networks. This may result in the violation of the physical limits of multi-energy networks, making the delivery of the services infeasible [10]. On the other hand, network-secure bids are computed by network-constrained bidding models, which can assume the form of centralized [11][12][13] or distributed [7][10] approaches. Centralized approaches consider the joint optimization of aggregator and network problems, while distributed approaches solve aggregator and network problems in a distributed manner, which allows preserving the data privacy of aggregators and distribution system operators (DSOs). Typically, distributed approaches use the alternating direction method of multipliers (ADMM) [7][10] to solve the aggregator and network problems separately. Moreover, centralized approaches use simplified electricity, gas, and heat network models (i.e., convex models) to make the joint aggregator and network problem solvable. These simplifications transform the non-convex solution space of the network problems into a convex space, which results many times in the reduction of the feasible space, or even in the expansion of the space to infeasible areas [14]. As a result, solutions can be infeasible or suboptimal in the original solution space. The decentralized approaches allow solving the original problem by breaking it down into smaller and less complex problems. In this way, the non-convex models of energy networks can be considered, which benefits the feasibility of the global optimization problem.

The second group of optimization algorithms is not so common in the literature. This group covers real-time optimization algorithms to deliver multi-energy services traded by aggregators in day-ahead markets. The real-time optimization algorithms optimize and control DMERs to deliver electricity market services, such as energy [15][16][17][18] and reserves [9][15][17][18]. Typically, they exploit MPC frameworks, which allow aggregators to reoptimize their DMER portfolios with the latest and most accurate dispatch and uncertainty data in real-time. This increases the reliability of the services and maximizes the profits of the aggregators by reducing imbalance penalties. In more detail, the optimization algorithms in [9] and [15] are network-free, while the other three [16][17][18] are network-secure from the electricity network perspective. The optimization algorithm [16] uses a centralized model to solve aggregator and network problems, while approaches [17] and [18] are distributed. The distributed approaches have the advantage of solving the privacy and computational challenges described previously.

The works described above together with other studies not covered here have provided valuable contributions to the formulation of algorithms to optimize DMERs for market participation. However, to our best knowledge, none of the studies in the literature proposes a real-time optimization algorithm to safely deliver multi-energy services traded by aggregators (i.e., delivering multi-energy services without violating network constraints) in electricity (energy and reserve), natural gas, green hydrogen, and carbon markets. More specifically, none of the works considers the real-time optimization of aggregators considering electricity, gas, and heat networks and a portfolio of associated DMERs. The joint consideration of all these technologies

and system constraints yields several benefits, in particular, the increase of flexibility and security of the energy system and an overall reduction of energy costs.

In addition to the research gaps described above, none of the works investigated the impacts of the aggregators adopting a green hydrogen policy. This is important for energy actors like aggregators to understand under what conditions the production of green hydrogen is economically attractive and what are the associated externalities.

1.3. Contributions and advantages of the proposed model

This paper proposes a new hierarchical MPC framework to support aggregators in the real-time delivery of network-secure and multi-energy services. The aim is to ensure that aggregators deliver cost-effectively and safely the multi-energy services traded in day-ahead electricity, gas, green hydrogen and carbon markets. The MPC framework uses the ADMM on a rolling horizon to negotiate the network-secure delivery of multi-energy services between aggregators and multi-energy DSOs. The multi-energy services include electricity (energy and reserve), natural gas, green hydrogen, and carbon allowances, which result from the real-time optimization of the multi-energy resources managed by aggregators.

This work builds upon a previous paper [7], extending it in two ways. Firstly, and most importantly, it completes the participation cycle of aggregators in multi-energy markets. In our previous work [7], we developed a network-secure bidding optimization model for the participation of aggregators in multi-energy day-ahead markets. In that work, the framework developed only considered the submission of day-ahead bids by the aggregators, without considering their real-time activation. This work concludes the entire cycle of multi-energy market participation, by addressing the real-time phase. It provides clear evidence of the effectiveness of the proposed approach, which, to the best of our knowledge, was never discussed before in the literature, namely concerning the advantages of considering network-secure bidding methods both in day-ahead and in real-time phases. Secondly, it extends the multi-energy markets framework by considering the aggregators' participation in green hydrogen markets, which is an innovative feature that cannot be found in the literature available.

Given the research gaps identified in the literature review, the main contributions of this new hierarchical MPC framework are the following:

1. It enables aggregators to safely deliver multi-energy services traded in day-ahead electricity, natural gas, green hydrogen, and carbon markets. To the best of our knowledge, this is the first work that proposes an approach to enable the network-secure delivery of multi-energy services traded in these four markets;
2. It optimizes for the first time a portfolio of DMERs considering the non-convex constraints of electricity, gas (with blending of natural gas and hydrogen) and heat networks. This ensures that the solution is feasible in the space of the combined energy networks and vectors. We can only ensure feasibility, if we use the non-convex constraints of the different energy networks. In addition, this also allows us to search for an "optimal" solution in the combined space of all networks and energy vectors, instead of searching for sub-optimal solutions in sub-spaces (in the cases where we consider fewer energy networks and energy vectors).

In addition to the contributions described above, the following studies using a real-world test case are also conducted:

1. The proposed hierarchical MPC was used to identify the adequate level of network observability that provides the most cost-effective and reliable solution to aggregators. In this study, we benchmark our approach against state-of-the-art approaches. As explained before, this study provides much relevant knowledge about the advantages of using network-secure frameworks in both day-ahead bidding and real-time delivery phases. This knowledge was lacking in the literature despite its utmost importance, as most of the network-secure frameworks developed and their studies would focus on the day-ahead bidding phase alone (e.g. [7][10]-[13]), disregarding the forecasting errors that naturally occur when forecasting day-ahead consumption, production and resources availability;
2. A series of sensitivity analyses were performed to evaluate the impacts for aggregators when adopting a green hydrogen policy under different price scenarios of green hydrogen and carbon prices.

1.4. Paper organization

The remaining paper is organized as follows. Section 2 describes the framework of the multi-energy aggregator. Section 3 describes the proposed hierarchical model predictive control. Sections 4 and 5 describe the optimization subproblems of the multi-energy aggregator and multi-energy DSOs. Sections 6 and 7 discuss the test case and results. Finally, section 8 presents the conclusions of the work.

2. Multi-energy aggregator framework

In this section, we describe the framework for a multi-energy aggregator to participate in electricity, natural gas, green hydrogen, and carbon markets. We also detail the relevant interactions of the aggregator with transmission system operators (TSOs), DSOs, market operators, and prosumers with multi-energy resources.

2.1. Interactions of the multi-energy aggregator with electricity, natural gas, green hydrogen, and carbon markets

The multi-energy aggregator participates in the electricity (energy and secondary reserve), natural gas, green hydrogen, and carbon markets of the Iberian Peninsula (Portugal and Spain). In the day-ahead stage, the aggregator behaves as a price-taker and submits demand (electricity), natural gas, hydrogen, and CO_2bids at cap prices, supply (electricity) and reserve bids at floor prices, so that all offers are accepted in the markets. In the real-time stage, the aggregator delivers the multi-energy services traded in day-ahead markets. It is important to note that the framework developed in this work can be easily adapted to other energy markets.

In the next subsections, we describe the framework of the electricity, natural gas, green hydrogen, and carbon markets. Then we discuss the steps of the aggregator in these markets.

2.1.1. Electricity markets

The aggregator participates in energy and secondary[3] reserve markets. In the day-ahead session of the energy market, the aggregator submits bids including price (€/MWh) and hourly quantity (MWh). The market operator collects and submits them to EUPHEMIA [19], a European market-clearing platform, to be dispatched. Then, the TSO of each control area runs congestion management [20] to calculate viable energy schedules within their control areas.

The day-ahead secondary reserve market begins after the congestion management stage. In this market, the TSO buys secondary reserve as regulation band (MW), considering the constraints

[3] Secondary reserve is also known as automatic frequency restoration reserve in Europe, and regulation reserve in the U.S. and Australia.

of the transmission network of its control area [21]. Secondary reserve is remunerated under the form of availability (€/MW), set in the secondary reserve market, and utilization (€/MWh), set in the tertiary reserve market.

In the real-time stage, the electricity TSO dispatches the secondary reserve through an automatic generation control (AGC) signal. Based on the AGC signal, the aggregator dispatches the DMERs to deliver the energy and secondary reserve traded in the day-ahead. The aggregator's transactions are settled days after delivery.

2.1.2. Natural gas market

In the day-ahead session of the natural gas market, the aggregator submits bids including price (€/MWh) and daily quantity (MWh/day). The market operator collects the bids and clears the market. Then, the gas TSO validates the bids, taking into account the technical constraints of the transmission gas network [22].

In the real-time stage, the aggregator delivers the natural gas traded in the day-ahead market by dispatching the DMERs. The gas transactions are settled days after delivery.

2.1.3. Green hydrogen market

The green hydrogen market is not fully developed in the Iberian Peninsula, nor in any other European country. In this paper, we assume that the green hydrogen market will present a similar framework to the natural gas market. In addition, we assume that the aggregator can buy renewable energy certificates, known as guarantees of origin in Europe, to ensure that the hydrogen traded by the aggregator is green. This certification scheme is in line with the new mechanisms being discussed today at the European level. However, it does not consider some of the additionality requirements related to the geographic and temporal correlations between renewable electricity generation and hydrogen production [23].

2.1.4. EU carbon market

The EU carbon market is an auction-based market that occurs three times per week where bidders submit bids to buy a specific number of allowances (in tonnes of CO_2) at a given price (€/tCO_2). The listed emitters of greenhouse emissions must cover their yearly emissions by buying allowances in this market. Facilities like CHPs, receive free allowances (calculated through benchmarking [24]) for the heat produced, although they still need to buy emission allowances for the electricity generated.

In this paper, we consider that the aggregator trades allowances in the day-ahead stage, and ensures that the allowances are respected in real-time by optimizing the operation of DMERs.

2.1.5. Chronological steps of the aggregator

The chronological steps of the aggregator in the four multi-energy markets described above are presented in Figure 1. In the day-ahead stage (day D-1), the aggregator begins by computing electricity (energy and secondary reserve), gas, green hydrogen, and CO_2bids. Afterwards, the aggregator submits the bids to the respective markets. The bids must be submitted before the gate closures of electricity (12h for energy, and 19h45 for secondary reserve), natural gas (9h30), green hydrogen (9h30), and carbon (11h) markets. In the real-time stage (day D), the aggregator delivers the multi-energy services traded in the day-ahead markets.

In this paper, we propose a new hierarchical MPC framework to support the actions of the aggregator during real-time. The calculation of day-ahead bids was addressed in this work [7].

2.2. Interactions of the multi-energy aggregator with the distribution system operators of electricity, gas, and heat networks

Today, the DSOs of electricity, gas, and heat networks do not participate in wholesale markets. This means that the bids submitted to the day-ahead markets or delivered in real-time are not validated by the DSOs, which may cause problems in distribution networks. To address this issue, we propose that the aggregator negotiates with DSOs network-secure services in both day-ahead and real-time stages. In this paper, we cover the real-time negotiation, which is described in detail in section 3. The day-ahead negotiation was covered in Ref. [7].

The real-time negotiation of the aggregator with DSOs assures that all the multi-energy services traded in day-ahead markets are delivered without affecting networks' normal operation and in compliance with their technical restrictions.

2.3. Interactions of the aggregator with the owners of the distributed multi-energy resources

The aggregator manages the DMERs of prosumers located in electricity, gas, and heat networks at the distribution level. All DMERs are flexible and include PVs, battery energy storage systems, heat pumps, thermal loads, CHPs, and hydrogen technologies (e.g., electrolyzers, hydrogen storage systems, fuel stations and fuel cells). The remaining electricity, gas and heat loads of the prosumers connected to the networks are inflexible and need to be supplied by the aggregator.

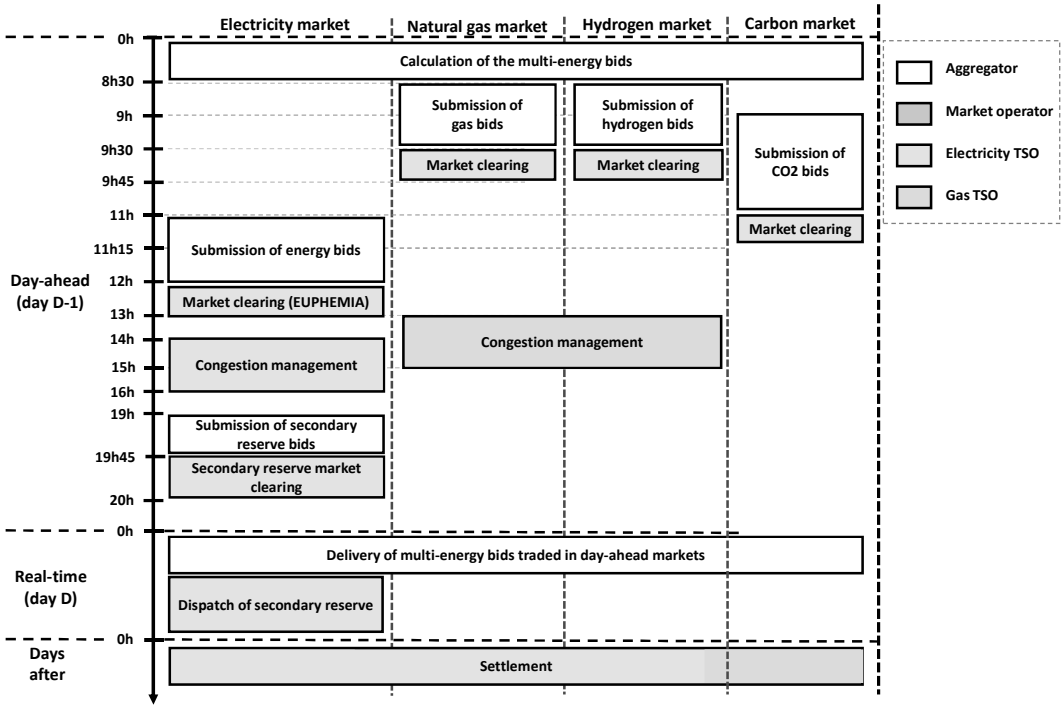

Figure 1 – Sequential steps of the aggregator in the electricity, natural gas, green hydrogen, and carbon markets

3. Hierarchical model predictive control framework

In this section, we present the hierarchical MPC framework used by the aggregator to safely deliver the multi-energy services (bids) traded in the day-ahead markets. The hierarchical MPC has two levels, as illustrated in Figure 2. In the first level, a multi-energy and network-secure optimization model computes network-secure bands[4] and control set-points for the DMERs. The optimization model is solved on a rolling horizon framework, which moves forward in intervals

[4] Bands define the flexibility of DMERs to increase/reduce generation/load.

of 1h for a horizon of 24h. In the second level, a controller adjusts the set-points (3) using the bands communicated by level 1 (1) to track the AGC signal (2) communicated by the TSO. The controller runs in cycles of 20s.

The level 1 of the hierarchical MPC framework is described in the next subsection. The controller used in level 2 was developed in previous work, and its description can be found in [16].

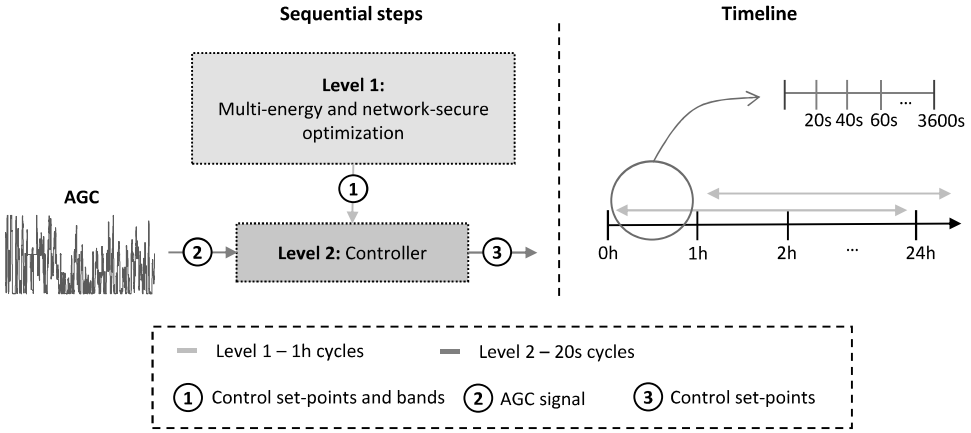

Figure 2 - Hierarchical model predictive control framework.

3.1. Level 1 - Multi-energy and network-secure optimization model

The generic formulation of the multi-energy and network-secure optimization problem is given by (1)-(4). The objective function (1) minimizes the net-cost of delivering the multi-energy services traded in day-ahead markets, without violating the constraints of the aggregator (2) and multi-energy DSOs (3). Constraint (4) is added here to enable the decomposition of the problem by the agent, as will be described in the next section. This constraint ensures the feasibility of the optimization problem. Let P^d be a copy of $\hat{P}^d$, and denote delivery scenarios[5] per energy vector $d \in \{E, G, H\}$ from aggregator and DSO perspectives, respectively. Let X and Y be the other variables of the aggregator and multi-energy DSOs.

$$\text{Min } f(P^E, P^G, P^H, X) \tag{1}$$

$$h(P^E, P^G, P^H, X) \leq 0 \tag{2}$$

$$g^d\left(\hat{P}^d,\ Y^d\right) \leq 0, \quad \forall\, d \in \{E, G, H\} \tag{3}$$

$$P^d - \hat{P}^d = 0, \qquad \forall\, d \in \{E, G, H\} \tag{4}$$

In this paper, we use the ADMM [25] to decompose the problem (1)-(4) into aggregator (5)-(6) and multi-energy DSO (8)-(9) subproblems and solve them. This allows solving the subproblem of each agent separately without violating their data privacy. In addition, it makes the problem (1)-(4) computationally tractable by decomposing it into smaller subproblems.

The ADMM solves the aggregator (5)-(6) and multi-energy DSO (8)-(9) subproblems iteratively until reaching a consensus solution. The ADMM includes three steps per iteration k, as illustrated in Figure 3.

In the first step, the aggregator solves its optimization subproblem (5)-(6) to compute control set-points, bands, and delivery scenarios P^d. The aggregator problem (5)-(6) is defined by the objective function (5) and constraints (6). The objective function (5) has two terms. The first term minimizes the net-cost of delivering the multi-energy services traded in day-ahead

[5] Delivery scenarios define possible exchanges of power between the aggregator and DSOs. Delivery scenarios are defined per network node.

markets. The second term is the augmented Lagrangian (7) applied to constraint (4). It is used to penalize the calculation of delivery scenarios that violate multi-energy network constraints. Let $\pi^{d,k}$ be the dual variables, and ρ be a scalar.

$$Min\ f(P^E, P^G, P^H, X) + \sum_{d\in\{E,G,H\}} \mathcal{L}^d(P^d, \hat{P}^{d,k}, \pi^{d,k}) \quad (5)$$

$$h(P^E, P^G, P^H, X) \leq 0 \quad (6)$$

$$\mathcal{L}^d(P^d, \hat{P}^d, \pi^d) = \pi^d\left(P^d - \hat{P}^d\right) + \frac{\rho}{2}\left\|P^d - \hat{P}^d\right\|_2^2 \quad (7)$$

In the second step, the DSO of each energy network solves its distribution network subproblem (8)-(9) to compute network-secure delivery scenarios $\hat{P}^d$. The distribution network problem of each DSO is defined by the objective function (8) and constraints (9). The objective function (8) penalizes the calculation of network-secure delivery scenarios that deviate from the preferences of the aggregator.

$$Min\ \mathcal{L}^d(P^{d,k+1}, \hat{P}^d, \pi^{d,k}) \quad (8)$$

$$g\left(\hat{P}^d, Y^d\right) \leq 0 \quad (9)$$

In the third step, an independent platform[6] computes dual variables $\pi^{d,k+1}$ through equation (10). The dual variables are prices used to penalize the calculation of delivery scenarios that either violate multi-energy network constraints or that deviate from the preferences of the aggregator. The three steps are repeated until the ADMM converges.

$$\pi^{d,k+1} = \pi^{d,k} + \rho\left(P^{d,k+1} - \hat{P}^{d,k+1}\right) \quad (10)$$

The ADMM converges when the stop criteria defined by residuals (11) and (12) are satisfied [25]. Let ϵ^{Abs} be the absolute tolerance and a the dimension of the residuals.

$$\left\|\left(P^{d,k+1} - \hat{P}^{d,k+1}\right)^T\right\|_2 \leq \epsilon^{Abs}\sqrt{a} \quad (11)$$

$$\left\|\rho\left(\hat{P}^{d,k+1} - P^{d,k+1}\right)^T\right\|_2 \leq \epsilon^{Abs}\sqrt{a} \quad (12)$$

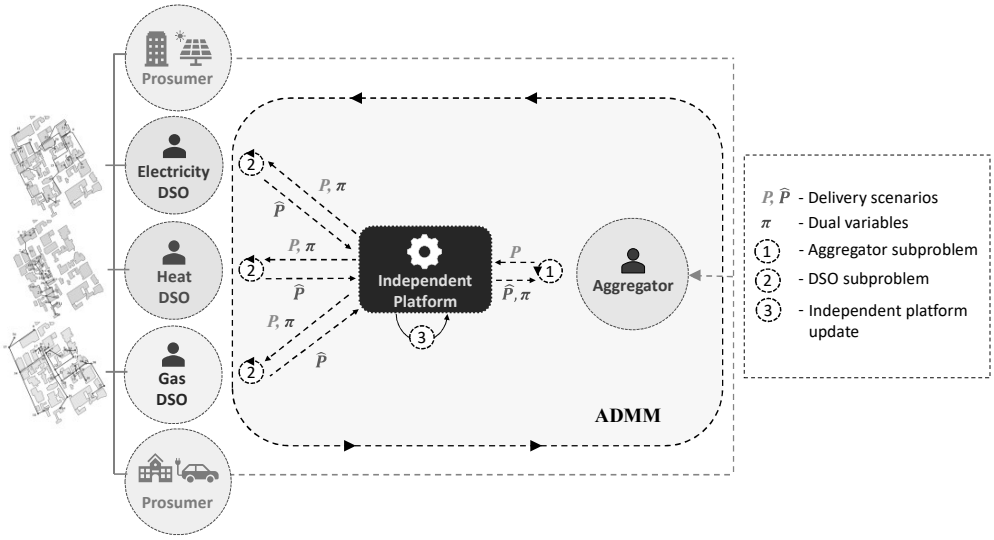

Figure 3 – ADMM algorithm.

[6] An independent platform is managed by an authorized third-party entity to ensure the data privacy of DSOs and the aggregator [42].

The optimization subproblems of the aggregator and DSOs were described in their generic form. In the next two sections, we describe in more detail these optimization subproblems.

4. Aggregator subproblem: operational optimization model

This section presents the optimization subproblem used by the aggregator to deliver the multi-energy bids traded in day-ahead electricity, natural gas, green hydrogen, and carbon markets. In more detail, the optimization subproblem computes bands, control set-points, and delivery scenarios.

4.1. Objective function

The objective function (13) minimizes the net-cost of the aggregator dispatching the electricity, natural gas, green hydrogen, and CO_2 traded in the day-ahead electricity (energy and secondary reserve), gas, green hydrogen, and carbon markets. The objective function (13) is divided into 8 terms. The first term (14) represents the real-time electricity costs – it includes the energy imbalance costs, secondary reserve mobilization net-costs, and penalties for not providing secondary reserve. The terms (15)-(20) represent the imbalance costs between day-ahead commitments and real-time deliveries of guarantees of origin (15), natural gas (16), green hydrogen (17) and its derivative products (water (18) and oxygen (19)), and CO_2 (20). The last term (21) represents the penalty term of the augmented Lagrangian, which penalizes the violation of the constraints of the electricity, gas, and heat networks.

$$Min \sum_{t\in T}\left[f_t^E + f_t^{GO} + \sum_{d\in\{E,G,H,H2\}}\sum_{s\in\{En,U,D\}}\sum_{n\in N^d}\mathcal{L}_{n,t}^{s,d}\right] + \sum_{v\in\{G,H2,H2O,O2,C\}} f^v \tag{13}$$

$$f_t^E = \left(\lambda_t^{E,-}\Delta P_t^{E,-} - \lambda_t^{E,+}\Delta P_t^{E,+}\right)\Delta t + (\lambda_t^D \phi_t^D D_t^E - \lambda_t^U \phi_t^U U_t^E)\Delta t + \lambda_t^{B,-}(\Delta U_t^E + \Delta D_t^E)\Delta t \tag{14}$$

$$f_t^{GO} = \lambda_t^{GO}\left(\Delta P_t^{GO,-} - \Delta P_t^{GO,+}\right)\Delta t \tag{15}$$

$$f^G = \lambda^G(\Delta P^{G,-} - \Delta P^{G,+})\Delta t \tag{16}$$

$$f^{H_2} = \lambda^{H_2}(\Delta P^{H_2,-} - \Delta P^{H_2,+})\Delta t \tag{17}$$

$$f^{H_2O} = \lambda^{H_2O}(\Delta P^{P2G,E,-} - \Delta P^{P2G,E,+})c^{H_2O}\Delta t \tag{18}$$

$$f^{O_2} = \lambda^{O_2}(\Delta P^{P2G,E,+} - \Delta P^{P2G,E,-})c^{O_2}\Delta t \tag{19}$$

$$f^C = \lambda^{CO_2}(\Delta P^{C,-} - \Delta P^{C,+})c^{CO_2,G}\Delta t \tag{20}$$

$$\mathcal{L}_{n,t}^{s,d} = \pi_{n,t}^{s,d}\left(P_{n,t}^{s,d} - \hat{P}_{n,t}^{s,d}\right) + \frac{\rho}{2}\left(P_{n,t}^{s,d} - \hat{P}_{n,t}^{s,d}\right)^2 \tag{21}$$

4.2. Multi-energy service constraints

Constraints (22)-(24) define the electricity (demand and supply), natural gas, and green hydrogen to be delivered in real-time. Constraints (25) and (26) define the upward and downward secondary reserves to be delivered in real-time. They include the flexibility provided by BESSs, PV systems, HPs, CHPs, electrolyzers, and fuel cells.

$$P_t^{E,RT} = \sum_{n\in N^E} P_{n,t}^{En,E}, \quad \forall\, t \in T \tag{22}$$

$$P_t^{G,RT} = \sum_{n\in N^{GL}} P_{n,t}^{En,G}, \quad \forall\, t \in T \tag{23}$$

$$P_t^{H_2,RT} = \sum_{n \in N^{H_2}} P_{n,t}^{En,H_2}, \quad \forall\, t \in T \tag{24}$$

$$U_t^E = \sum_{j \in J}\left(U_{j,t}^{Sto,+} + U_{j,t}^{Sto,-} + U_{j,t}^{PV} + U_{j,t}^{HP} + U_{j,t}^{CHP,E} + U_{j,t}^{P2G,E} + U_{j,t}^{FC,E}\right), \quad \forall\, t \in T \tag{25}$$

$$D_t^E = \sum_{j \in J}\left(D_{j,t}^{Sto,+} + D_{j,t}^{Sto,-} + D_{j,t}^{PV} + D_{j,t}^{HP} + D_{j,t}^{CHP,E} + D_{j,t}^{P2G,E} + D_{j,t}^{FC,E}\right), \quad \forall\, t \in T \tag{26}$$

Constraints (27) and (28) define natural gas imbalances caused by the expected activation of secondary reserve provided by CHPs. Constraints (29) and (30) define green hydrogen imbalances caused by the expected activation of secondary reserve provided by electrolyzers (P2G).

$$U_t^G = \sum_{j \in J} U_{j,t}^{CHP,G}, \quad \forall\ t \in T \tag{27}$$

$$D_t^G = \sum_{j \in J} D_{j,t}^{CHP,G}, \quad \forall\ t \in T \tag{28}$$

$$U_t^{H_2} = \sum_{j \in J} U_{j,t}^{P2G,Net,H_2}, \quad \forall\ t \in T \tag{29}$$

$$D_t^{H_2} = \sum_{j \in J} D_{j,t}^{P2G,Net,H_2}, \quad \forall\ t \in T \tag{30}$$

4.3. Imbalance constraints

Constraints (31)-(36) define imbalances between day-ahead market commitments and real-time expected realizations. In more detail, constraints (31)-(32) define hourly imbalances of electricity and guarantees of origin, and constraints (33)-(36) define daily imbalances of natural gas (33), green hydrogen (34)-(35), and CO_2 (36).

$$\Delta P_t^{E,-} - \Delta P_t^{E,+} = P_t^{E,RT} - P_t^{E,DA}, \forall\, t \in T \tag{31}$$

$$\Delta P_t^{GO,-} - \Delta P_t^{GO,+} = P_t^{GO,RT} - P_t^{GO,DA}, \forall\, t \in T \tag{32}$$

$$\Delta P^{G,-} - \Delta P^{G,+} = \sum_{t \in T}\left(P_t^{G,RT} + \phi_t^U U_t^G - \phi_t^D D_t^G\right) - P^{G,DA} \tag{33}$$

$$\Delta P^{H_2,+} - \Delta P^{H_2,-} = \sum_{t \in T}\left(P_t^{H_2,RT} + \phi_t^D D_t^{H_2} - \phi_t^U U_t^{H_2}\right) - P^{H2,DA} \tag{34}$$

$$\Delta P^{P2G,E,-} - \Delta P^{P2G,E,+} = \sum_{j \in J}\sum_{t \in T}\left(P_{j,t}^{P2G,E} + \phi_t^D D_{j,t}^{P2G,E} - \phi_t^U U_{j,t}^{P2G,E}\right) - P^{P2G,E,DA} \tag{35}$$

$$\Delta P^{C,-} - \Delta P^{C,+} = \frac{\mathrm{A}^{+,CO_2}}{c^{CO_2,G}\Delta t} + \sum_{j \in J}\sum_{t \in T}\left(P_{j,t}^{CHP,E} + U_{j,t}^{CHP,E}\phi_t^U - D_{j,t}^{CHP,E}\phi_t^D\right) - P^{C,DA} \tag{36}$$

$$\Delta P_t^{E,-}, \Delta P_t^{E,+}, \Delta P_t^{GO,-}, \Delta P_t^{GO,+}, \geq 0, \forall\, t \in T \tag{37}$$

$$\Delta P^{G,-}, \Delta P^{G,+}, \Delta P^{H_2,-}, \Delta P^{H_2,+}, \Delta P^{P2G,E,-}, \Delta P^{P2G,E,+}, \Delta P^{C,-}, \Delta P^{C,+} \geq 0 \tag{38}$$

Constraints (39) and (40) ensure that the aggregator only provides secondary reserve when electricity imbalances are not expected to occur. Constraints (41) and (42) define the secondary reserve band not supplied.

$$\Delta P_t^{E,-} + \Delta P_t^{E,+} \leq (1 - b_t^E)M, \forall\, t \in T \tag{39}$$

$$D_t^E + U_t^E \leq b_t^E(D_t^{E,DA} + U_t^{E,DA}), \forall\, t \in T \tag{40}$$

$$\Delta D_t^E = D_t^{E,DA} - D_t^E, \forall\, t \in T \tag{41}$$

$$\Delta U_t^E = U_t^{E,DA} - U_t^E, \forall\, t \in T \tag{42}$$

$$D_t^E, U_t^E, \Delta D_t^E, \Delta U_t^E \geq 0, \forall\, t \in T \tag{43}$$

4.4. Market regulation constraints

The rules of the secondary reserve market (in the Portuguese control area) define that upward and downward bands should be 2/3 and 1/3 of the total band, as represented by constraint (44) [4].

$$U_t^E = 2.D_t^E, \forall\, t \in T \tag{44}$$

Constraint (45) defines the CO_2 allowances to cover the electricity generated by the CHPs. Note that CHPs receive free allowances for the heat produced, although they still need to buy CO_2 allowances for the electricity generated.

$$\mathrm{A}^{+,CO_2} - \mathrm{A}^{-,CO_2} = \sum_{t\in T}\sum_{j\in J}[(P_{j,t}^{CHP,H} + U_{j,t}^{CHP,H}\phi_t^U - D_{j,t}^{CHP,H}\phi_t^D)c^{CO_2,G}\Delta t] - FA^{CO_2} \tag{45}$$

$$\mathrm{A}^{+,CO_2}, \mathrm{A}^{-,CO_2} \geq 0 \tag{46}$$

Constraint (47) defines the guarantees of origin bought and sold by the aggregator. The aggregator buys when the renewable energy resources managed by it do not produce enough electricity to certify the hydrogen produced by the electrolyzers as green. The aggregator sells when the opposite happens.

$$P_t^{GO,RT} = \sum_{j\in J} P_{j,t}^{P2G,E} - \sum_{j\in J} P_{jt}^{PV} + \sum_{j\in J}\left(D_{j,t}^{P2G,E} + D_{j,t}^{PV}\right)\phi_t^D - \sum_{j\in J}\left(U_{j,t}^{P2G,E} + U_{j,t}^{PV}\right)\phi_t^U, \quad \forall \quad t \in T \tag{47}$$

4.5. Delivery scenario constraints

Delivery scenarios define possible exchanges of power between the aggregator and multi-energy networks (or multi-energy DSOs). In the ADMM negotiation, they are used by the DSOs to check for network violations caused by the delivery of aggregator services.

We model twelve delivery scenarios. The first six scenarios model the delivery of services traded in the day-ahead markets, such as electricity (48), natural gas (49), heat (50), hydrogen (51), and secondary reserve (52)-(53). The last six scenarios model imbalances in heat (54)-(55) and gas (56)-(59) networks caused by the activation of secondary reserve.

Constraint (48) defines the electricity delivery scenario, which results from the electricity consumed by BESSs, HPs, inflexible loads and electrolyzers, and electricity generated by CHPs, BESSs, PV systems, and fuel cells.

$$P_{n,t}^{En,E} = \sum_{j\in J_n}(P_{j,t}^{Sto,+} + P_{j,t}^{HP} + P_{j,t}^{IL,E} + P_{j,t}^{P2G,E} - P_{j,t}^{CHP,E} - P_{j,t}^{Sto,-} - P_{jt}^{PV} - P_{j,t}^{FC,E}), \quad \forall\, n \in N^E, t \in T \tag{48}$$

Constraint (49) defines the gas delivery scenario, which results from the gas consumed by CHPs and inflexible loads.

$$P_{n,t}^{En,GL} = \sum_{j\in J_n}(P_{j,t}^{CHP,G} + P_{j,t}^{IL,G}), \forall\, n \in N^{GL}, \quad t \in T \tag{49}$$

Constraint (50) defines the heat delivery scenario, which results from the heat consumed by flexible and inflexible heating loads connected to the district heating, and the heat generated by CHPs.

$$P_{n,t}^{En,H} = \sum_{j\in J_n}(P_{j,t}^{DH} + P_{j,t}^{IL,H} - P_{j,t}^{CHP,H}), \forall\, n \in N^H, \quad t \in T \tag{50}$$

Constraint (51) defines the hydrogen delivery scenario, which results from the hydrogen injected into the gas network by hydrogen technologies.

$$P_{n,t}^{En,H_2} = \sum_{j \in J_n} (P_{j,t}^{P2G,Net,H_2} + P_{j,t}^{Sto,Net,H_2}), \forall\, n \in N^{H_2},\ \ t \in T \tag{51}$$

Constraints (52) and (53) define the secondary reserve delivery scenarios in both upward (52) and downward (53) directions. They are provided by CHPs, BESSs, fuel cells, HPs, PV systems and electrolyzers.

$$P_{n,t}^{U,E} = P_{n,t}^{E} - \sum_{j \in J_n} \left(U_{j,t}^{CHP,E} + U_{j,t}^{Sto,+} + U_{j,t}^{Sto,-} + U_{j,t}^{FC,E} + U_{j,t}^{HP} + U_{j,t}^{PV} + U_{j,t}^{P2G,E}\right),\ \ \forall\, n \in N^E, t \in T \tag{52}$$

$$P_{n,t}^{D,E} = P_{n,t}^{E} + \sum_{j \in J_n} \left(D_{j,t}^{CHP,E} + D_{j,t}^{Sto,+} + D_{j,t}^{Sto,-} + D_{j,t}^{FC,E} + D_{j,t}^{HP} + D_{j,t}^{PV} + D_{j,t}^{P2G,E}\right),\ \ \forall\, n \in N^E, t \in T \tag{53}$$

Constraints (54) and (55) define the scenarios of heat imbalances caused by the possible activation of the secondary reserve provided by district heating loads and CHPs.

$$P_{n,t}^{U,H} = P_{n,t}^{H} - \sum_{j \in J_n} \left(U_{j,t}^{DH} + U_{j,t}^{CHP,H}\right),\ \ \forall\, n \in N^H, t \in T \tag{54}$$

$$P_{n,t}^{D,H} = P_{n,t}^{H} - \sum_{j \in J_n} \left(D_{j,t}^{DH} + D_{j,t}^{CHP,H}\right),\ \ \forall n \in N^H, t \in T \tag{55}$$

Constraints (56) and (57) define the scenarios of gas imbalances caused by the possible activation of the secondary reserve provided by CHPs.

$$P_{n,t}^{U,GL} = P_{n,t}^{G} + \sum_{j \in J_n} \left(U_{j,t}^{CHP,G}\right),\ \ \forall\, n \in N^{GL}, t \in T \tag{56}$$

$$P_{n,t}^{D,GL} = P_{n,t}^{G} - \sum_{j \in J_n} \left(D_{j,t}^{CHP,G}\right),\ \ \forall\, n \in N^{GL}, t \in T \tag{57}$$

Constraints (58) and (59) define the scenarios of hydrogen imbalances caused by the possible activation of the secondary reserve provided by electrolyzers.

$$P_{n,t}^{U,H_2} = P_{n,t}^{H_2} - \sum_{j \in J_n} \left(U_{j,t}^{P2G,Net,H_2}\right),\ \ \forall\, n \in N^{H_2}, t \in T \tag{58}$$

$$P_{n,t}^{D,H_2} = P_{n,t}^{H_2} + \sum_{j \in J_n} \left(D_{j,t}^{P2G,Net,H_2}\right),\ \ \forall\, n \in N^{H_2}, t \in T \tag{59}$$

4.6. Distributed multi-energy resource constraints

In this paper, we consider PVs, battery energy storage systems, CHPs, heat pumps, district heating loads, and hydrogen technologies as DMERs. The next subsection details the constraints of hydrogen technologies. The constraints of the remaining technologies are described in Appendix A to improve the readability of the main body of the paper.

We prioritize the description of hydrogen technologies in the main body of the paper since it is one of the main contributions of this paper. The other technologies were described in Ref. [7].

4.6.1. Hydrogen technologies

Hydrogen technologies include electrolyzers, fuel stations, hydrogen storage systems, and fuel cells. Figure 4 illustrates an example of a green hydrogen hub with the mentioned technologies. In this hub, the electrolyzer produces green hydrogen by consuming renewable electricity from the grid (with guarantees of origin) or using local renewable energy resources managed by the aggregator. Afterwards, the green hydrogen can be injected into the gas network, stored, or consumed by a fuel station. The stored hydrogen can be later injected into the gas network or used to power a fuel cell or a fuel station.

The next four subsections describe the equations used to model green hydrogen hubs, like the one illustrated in Figure 4.

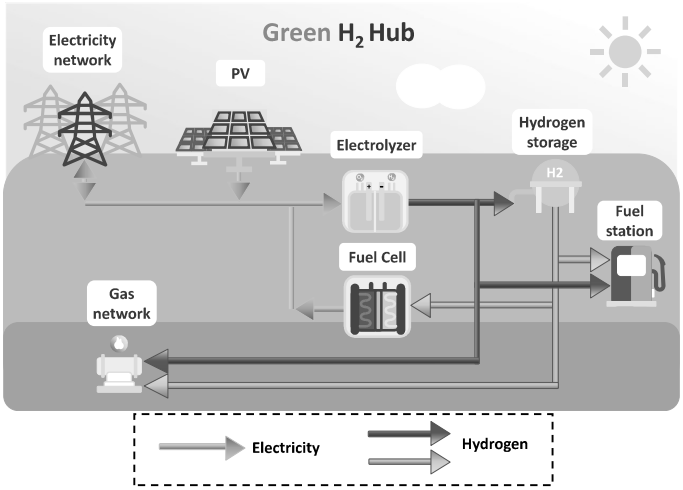

Figure 4 – Green hydrogen hub.

4.6.1.1. Electrolyzer constraints

Constraints (60)-(68) model the electrolyzers (P2G) connected to the electricity network. Constraints (60) and (61) define the hydrogen produced by the electrolyzers. Constraints (62)-(68) define the limits of the electrolyzers, (62) for electricity consumption and (63)-(68) for secondary reserve provision in upward and downward directions. The sign → represents the power that flows from X to Y. For example, the notation in $P2G \rightarrow Sto, H_2$ represents the hydrogen that flows from the electrolyzer to the hydrogen storage system.

$$P_{j,t}^{P2G,H_2} = \eta_j^{P2G} P_{j,t}^{P2G,E}, \quad \forall\ j \in J,\ \ t \in T \tag{60}$$

$$P_{j,t}^{P2G,H_2} = P_{j,t}^{P2G \rightarrow HV,H_2} + P_{j,t}^{P2G \rightarrow Net,H_2,} + P_{j,t}^{P2G \rightarrow Sto,H_2}, \quad \forall\ j \in J,\ \ t \in T \tag{61}$$

$$\underline{P^{P2G,E}} \leq P_{j,t}^{P2G,E} \leq \overline{P^{P2G,E}}, \quad \forall\ j \in J,\ \ t \in T \tag{62}$$

$$U_{j,t}^{P2G,E} \leq P_{j,t}^{P2G,E} - \underline{P_{j,t}^{P2G,E}}, \quad \forall\ j \in J,\ \ t \in T \tag{63}$$

$$D_{j,t}^{P2G,E} \leq \overline{P_{j,t}^{P2G,E}} - P_{j,t}^{P2G,E}, \quad \forall\ j \in J,\ \ t \in T \tag{64}$$

$$U_{j,t}^{P2G,H_2} = \eta_j^{P2G} U_{j,t}^{P2G,E}, \quad \forall\ j \in J,\ \ t \in T \tag{65}$$

$$D_{j,t}^{P2G,H_2} = \eta_j^{P2G} D_{j,t}^{P2G,E}, \quad \forall\ j \in J,\ \ t \in T \tag{66}$$

$$U_{j,t}^{P2G,H_2} = U_{j,t}^{P2G \rightarrow Net,H_2} + U_{j,t}^{P2G \rightarrow Sto,H_2}, \quad \forall\ j \in J,\ \ t \in T \tag{67}$$

$$D_{j,t}^{P2G,H_2} = D_{j,t}^{P2G \rightarrow Net,H_2} + D_{j,t}^{P2G \rightarrow Sto,H_2}, \quad \forall\ j \in J,\ \ t \in T \tag{68}$$

4.6.1.2. Hydrogen storage system constraints

Constraints (69)- (81) define the operation of hydrogen storage systems. Constraints (69) and (70) define the state-of-charge and its limits. Constraints (71)-(75) set the charging and discharging power and their limits. Binary variables $b^{Sto,H_2,+}$ and $b^{Sto,H_2,-}$ define if the hydrogen storage is in charging or discharing mode.

$$SOC_{j,t+1}^{Sto,H_2} = SOC_{j,t}^{Sto,H_2} + \left(P_{j,t}^{Sto,H_2,+} \eta_j^{Sto,H_2,-} - \frac{P_{j,t}^{Sto,H_2,-}}{\eta_j^{Sto,H_2,-}} \right) \Delta t - \gamma_j . SOC_{j,t}^{Sto,H_2}, \quad \forall\ \ j \in J,\ \ t \in T \tag{69}$$

$$\underline{SOC_j^{Sto,H_2}} \leq SOC_{j,t}^{Sto,H_2} \leq \overline{SOC_j^{Sto,H_2}}, \ \forall\ j \in J, \ t \in T \quad (70)$$

$$P^{Sto,H_2,+} = P_{j,t}^{P2G \to Sto,H_2}, \qquad \forall \quad j \in J, \ t \in T \quad (71)$$

$$P^{Sto,H_2,-} = P^{Sto \to HV,H_2} + P_{j,t}^{Sto \to Net,H_2} + P_{j,t}^{Sto \to FC,H_2}, \qquad \forall \quad j \in J, \ t \in T \quad (72)$$

$$\underline{P}^{Sto,H_2} \leq b^{Sto,H_2,+}.P_{j,t}^{Sto,H_2,+}, \ \forall\ j \in J, \ t \in T \quad (73)$$

$$P_{j,t}^{Sto,H_2,-} \leq b^{Sto,H_2,-}.\overline{P^{Sto,H_2,-}}, \ \forall\ j \in J, \ t \in T \quad (74)$$

$$b^{Sto,H_2,+} + b^{Sto,H_2,-} \leq 1, \ \forall\ j \in J, \ t \in T \quad (75)$$

Constraints (76)- (81) define the secondary reserve bands provided by the hydrogen storage systems. Constraints (76)-(79) define the power limits, while constraints (80) and (81) set the energy limits of hydrogen storage systems.

$$0 \leq D_{j,t}^{P2G \to Sto,H_2} \leq \overline{P^{Sto,H_2}} - P_{j,t}^{Sto,H_2,+}, \ \forall\ j \in J, \ t \in T \quad (76)$$

$$0 \leq U_{j,t}^{P2G \to Sto,H_2} \leq P_{j,t}^{Sto,H_2,+}, \ \forall\ j \in J, \ t \in T \quad (77)$$

$$0 \leq D_{j,t}^{Sto \to FC,H_2} \leq P_{j,t}^{Sto,FC,H_2}, \ \forall\ j \in J, \ t \in T \quad (78)$$

$$0 \leq U_{j,t}^{Sto \to FC,H_2} \leq \overline{P^{Sto,H_2}} - P_{j,t}^{Sto,H_2,-}, \ \forall\ j \in J, \ t \in T \quad (79)$$

$$D_{j,t}^{P2G \to Sto,H_2} + D_{j,t}^{Sto \to FC,H_2} \leq \frac{\overline{SOC_j^{Sto,H_2}} - SOC_{j,t+1}^{Sto,H_2}}{\Delta t}, \ \forall\ j \in J, \ t \in T \quad (80)$$

$$U_{j,t}^{P2G \to Sto,H_2} + U_{j,t}^{Sto \to FC,H_2} \leq \frac{SOC_{j,t+1}^{Sto,H_2} - \underline{SOC_j^{Sto,H_2}}}{\Delta t}, \ \forall\ j \in J, \ t \in T \quad (81)$$

4.6.1.3. Fuel cell constraints

Constraints (82)-(88) define the operation of the fuel cells. Constraints (82) and (83) define the electricity produced by the fuel cells. The remaining constraints (84)-(88) define the secondary reserve bands provided by the fuel cells.

$$P_{j,t}^{FC,E} = \eta_j^{FC}.P_{j,t}^{Sto \to FC,H_2}, \ \forall\ j \in J, \ t \in T \quad (82)$$

$$0 \leq P_{j,t}^{Sto \to FC,H_2} \leq b^{Sto,H_2,-}.\overline{P_j^{FC,H_2}}, \ \forall\ j \in J, \ t \in T \quad (83)$$

$$U_{j,t}^{Sto \to FC,H_2} \leq b^{Sto,H_2,-}.\overline{P_j^{FC,H_2}} - P_{j,t}^{Sto \to FC,H_2}, \ \forall\ j \in J, \ t \in T \quad (84)$$

$$D_{j,t}^{Sto \to FC,H_2} \leq P_{j,t}^{Sto \to FC,H_2}, \ \forall\ j \in J, \ t \in T \quad (85)$$

$$U_{j,t}^{FC,E} = \eta_j^{FC} U_{j,t}^{Sto \to FC,H_2}, \ \forall\ j \in J, \ t \in T \quad (86)$$

$$D_{j,t}^{FC,E} = \eta_j^{FC} D_{j,t}^{Sto \to FC,H_2}, \ \forall\ j \in J, \ t \in T \quad (87)$$

$$D_{j,t}^{FC,E}, U_{j,t}^{FC,E} \geq 0, \ \forall\ j \in J, \ t \in T \quad (88)$$

4.6.1.4. Fuel station constraint

Constraint (89) ensures that fuel stations supply hydrogen to inflexible loads, such as hydrogen vehicles. Note that the production of green hydrogen to supply fuel stations connected to local hubs is not traded in the market.

$$P_{j,t}^{P2G \to HV,H_2} + P_{j,t}^{Sto \to HV,H_2} = P_{j,t}^{HV}, \ \forall j \in J, t \in T \quad (89)$$

5. Distribution system operator subproblems: multi-energy flow optimization models

This section presents the multi-energy flow optimization models used by the DSOs to evaluate the network feasibility of the multi-energy market services expected to be delivered by the aggregator.

The multi-energy flow optimization models are decomposed by time step $t \in T$ and delivery scenario $s \in \{En, U, D\}$ (see section 4.5) and solved independently. This is possible because they are no dependencies between time steps and delivery scenarios in these problems. As a result, the subscripts of time and delivery scenarios are dropped in this section.

The next subsection describes the gas flow optimization problem used by the gas DSO to manage the flows of natural gas and hydrogen. The electricity and heat flow optimization problems are described in Appendix B to improve the readability of the main body of the paper. We prioritize the description of the gas flow optimization problem since hydrogen flow is one important innovation of this work. The other energy flow formulations were described in Ref. [7].

5.1. Gas flow optimization model

The gas flow optimization problem (90)-(104) is used by the gas DSO to assure that delivery scenarios of hydrogen and natural gas computed by the aggregator are network-secure.

5.1.1. Objective function

The objective function (90) minimizes the augmented Lagrangian penalty, which penalizes the calculation of network-secure gas delivery scenarios that deviate from the aggregator's preferences.

$$Min \sum_{d \in \{GL, H_2\}} \left[\sum_{m \in N^d} \pi_m^d \left(P_m^d - \hat{P}_m^d\right) + \frac{\rho}{2} \left(P_m^d - \hat{P}_m^d\right)^2 \right] \quad (90)$$

5.1.2. Network constraints

Constraints (91)-(92) define the limits of natural gas injection (91) and nodal pressure (92).

$$\underline{P_m^{NG}} \leq P_m^{NG} \leq \overline{P_m^{NG}}, \ \forall m \in N^{NG} \quad (91)$$

$$\underline{p_m^G} \leq p_m^G \leq \overline{p_m^G}, \ \forall m \in N^G \quad (92)$$

Constraint (93) models the gas balance in each node. Constraints (94)-(96) define the volumetric flow of natural gas (94), hydrogen (95), and gas mixture (96). c^{H_2} converts kWh to m3/h.

$$q_m^{NG} + \hat{q}_m^{H2} - \hat{q}_m^G + \sum_{n:n \to m} q_{n,m} - \sum_{n:m \to n} q_{m,n} = 0, \ \forall m \in N^G \quad (93)$$

$$q_m^{NG} = \frac{P_m^{NG}}{c^G}, \forall m \in N^{NG} \quad (94)$$

$$\hat{q}_m^{H_2} = \frac{\hat{P}_m^{H_2}}{c^{H_2}}, \forall m \in N^{H_2} \quad (95)$$

$$\hat{q}_m^G = \frac{\hat{P}_m^G . HHV_m^G}{\left(HHV_m^{Mix}\right)^2 c^G}, \forall m \in N^{GL} \quad (96)$$

Constraints (97)-(100) define the higher heating value (HHV) (97)-(98) and the relative gas density to air (99) of the gas mixture of hydrogen with natural gas [26]. Constraint (100) defines the fraction of hydrogen in the gas mixture.

$$HHV_m^{mix} = w_m^{H_2} HHV_m^{H_2} + \left(1 - w_m^{H_2}\right) HHV_m^G, \ \forall m \in N^G \quad (97)$$

$$\underline{HHV^{mix}} \leq HHV_m^{mix} \leq \overline{HHV^{mix}}, \ \forall m \in N^G \quad (98)$$

$$S_m^{mix} = w_m^{H_2} S_m^{H_2} + \left(1 - w_m^{H_2}\right) S_m^G, \ \forall m \in N^G \quad (99)$$

$$w_m^{H_2} = \frac{\hat{q}_m^{H_2}}{q_m^{NG} + \hat{q}_m^{H_2}}, \ \forall m \in N^G \quad (100)$$

Constraints (101)-(102) are related to the Wobbe Index (WI) [27] of the gas mixture. These two constraints are used to ensure that the energy output of the gas mixture is acceptable for the end-users and meet established quality of service requirements.

$$WI_m = \frac{HHV_m^{mix}}{\sqrt{S_m^{mix}}}, \ \forall m \in N^G \quad (101)$$

$$\underline{WI} \leq WI_m \leq \overline{WI}, \ \forall m \in N^G \quad (102)$$

Constraint (103) defines the steady-stage gas flow [28]. In this case, the gas flowing into the pipeline is equal to the gas flowing out of the pipeline. Constraint (104) defines the resistance coefficient of each pipeline.

$$(p_m^G)^2 - (p_n^G)^2 = K_{m,n}^G q_{m,n} \left|\left(q_{m,n}\right)^{0.848}\right|, \ \forall \ (m,n) \in B^G \quad (103)$$

$$K_{m,n}^G = \frac{(p^{G,St})^2 (S_m^{Mix})^{0.848} \theta^G}{57.3 \times 10^{-8} (\theta^{G,St})^2 143.52} \cdot \frac{L_{m,n}}{\left(\eta_{m,n}\right)^2 \left(d_{m,n}\right)^{4.848}}, \ \forall (m,n) \in B^G \quad (104)$$

6. Test case

We use the microgrid from the University of Manchester [29], as test case. This system was chosen due to the unavailability of suitable test cases in the Iberian Peninsula. Nonetheless, the framework developed can be applied to any microgrid independently of its geographical location. The microgrid is characterized by electricity, gas, and heat networks, as illustrated in Figure 5. The data of the case study is described in detail in the next 2 subsections. The data not explicitly provided here can be shared upon request.

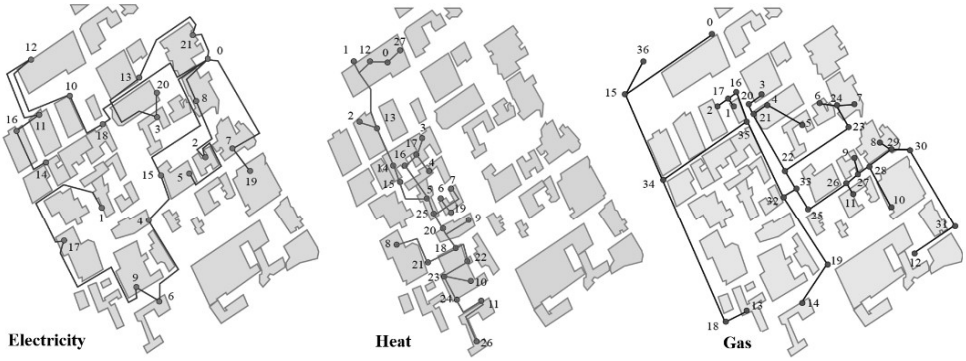

Figure 5 - Electricity, heat and gas networks of the study case [29].

6.1. DMER and network data

The DMERs are connected to the electricity, gas, and heat networks. The DMERs connected to the electricity network are 6 PVs, 5 BESSs, 5 HPs, and 2 CHPs. The DMERs connected to the gas network are 2 CHPs. The DMERS connected to the heat network are 2 CHPs and 5 district heating flexible loads. In addition to the mentioned DMERs, a green hydrogen hub is connected to electricity and gas networks at nodes 12 and 0, respectively. The green hydrogen hub has 1 electrolyzer, 1 fuel cell, 1 hydrogen storage system, 1 fuel station, and 1 PV.

The parameters and the network location of the PVs, BESSs, HPs, and CHPs can be found in [7]. The parameters of the hydrogen technologies are the following: an electrolyzer with a maximum power of 1500 kW and an efficiency of 0.6; hydrogen storage with a maximum power of 1000 kW, a minimum capacity of 400 kWh, a maximum capacity of 7900 kWh, and a self-discharging factor of 0.01%; a fuel cell with a maximum power of 250 kW, and an efficiency of 0.6; a fuel station with daily consumption of 150 kg of hydrogen.

The data on the electricity, heat and gas networks was sourced from [29]. In addition to this data, it was also considered the following gas network parameters: WI bounds of [45.7, 55.9] MJ/m^3 [30]; HHV bounds of [35.5, 47.8] MJ/m^3 [30]; network pressure of 2 bar.

6.2. Market data

The electricity market data includes hourly energy prices, imbalance prices, secondary reserve prices, upward and downward tertiary reserve prices, AGC signal, ratios of upward and downward mobilizations. Figure 6 illustrates the market data sourced from [31][32]. More information about the AGC signal used in this paper can be found in [15].

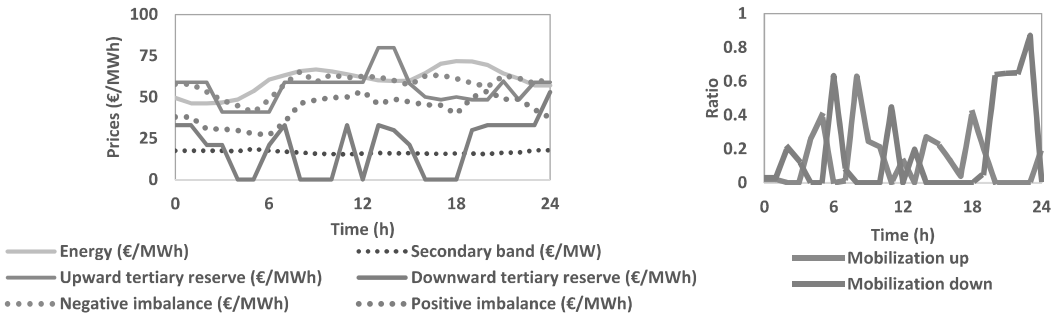

Figure 6 - Electricity market prices.

The natural gas, green hydrogen, and carbon markets have daily prices. The gas market data includes a gas price of 13.99€/MWh and a gas imbalance price of 13.34 €/MWh [33]. The green hydrogen market includes a hydrogen price of 73 €/MWh, hydrogen imbalance price of 76 €/MWh, a water price of 3.76 €/L, and oxygen price of 0.15 €/kg. We considered a carbon price of 25 €/tCO_2 and the price for the guarantees of origin was set at 0.56 €/MWh. It is worth mentioning that in subsection 7.2, we use different carbon prices [50, 200] €/tCO_2 and green hydrogen prices [25, 100] €/MWh to study the impact of different values on the economic performance of the aggregator.

7. Results

In this section, we discuss the economic, network, and computational performances of different combinations of day-ahead and real-time optimization strategies. The day-ahead and real-time optimization strategies vary on the level of multi-energy network observability. The combination of day-ahead and real-time optimization strategies are the following:

1. Day-ahead network-free and real-time network-free (NF-NF): the aggregator performs day-ahead and real-time optimizations using network-free approaches, which do not consider the constraints of the multi-energy networks of the DSOs;
2. Day-ahead network-free and real-time network-secure (NF-NS): the aggregator performs day-ahead optimization without considering multi-energy network constraints, and real-time optimization considering multi-energy network constraints;

3. Day-ahead network-secure and real-time network-free (NS-NF): the aggregator performs day-ahead optimization considering multi-energy network constraints, and real-time optimization without considering multi-energy network constraints;
4. Day-ahead network-secure and real-time network-secure (NS-NS): the aggregator performs day-ahead and real-time optimizations considering multi-energy network constraints. Note that the real-time network-secure strategy corresponds to the new hierarchical MPC proposed in this paper;

This section is divided into two main subsections. The first one, 7.1, presents and discusses the performance of the day-ahead and real-time optimization strategies. The second subsection, 7.2, discusses the impacts on the aggregator of adopting a green hydrogen policy under different price scenarios of green hydrogen and carbon prices.

The code data will become open-source and available before the end of the project (August 2023). This information will be made available in [34][35].

7.1. Comparison of day-ahead and real-time strategies

This subsection reports and discusses the day-ahead (7.1.1), real-time (7.1.2), and combined day-ahead and real-time results (7.1.3).

7.1.1. Day-ahead results

The aggregator participates in the day-ahead electricity (energy and secondary reserve), natural gas, green hydrogen, and carbon markets, as described in section 2. The aggregator computes bids using a bidding optimization model, which can be network-free (NF) or network-secure (NS). These two bidding optimization models are described and discussed in detail in Ref. [7].

The aim of this subsection is to discuss the day-ahead bidding results, which are used as inputs of the hierarchical MPC framework proposed in this paper to perform real-time optimization.

The results of Figure 7 and Table 1 show that NF and NS strategies result in the computation of different hourly and daily bids. These differences are caused by the imposition of the multi-energy networks' constraints. It means that the bids computed by NF are network-infeasible and could not be delivered since they would cause violations of the networks' constraints. The next subsection, 7.1.2, discusses the impact of these two day-ahead bidding strategies on the real-time performance of the aggregator.

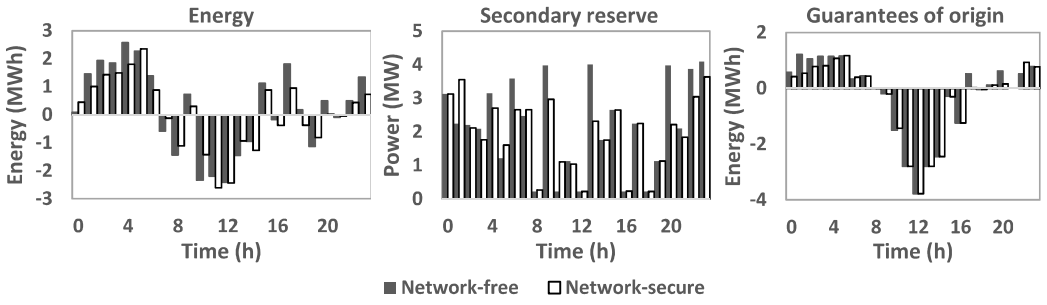

Figure 7 - Day-ahead hourly electricity (energy and reserve) and guarantees of origin bids. Positive values are reserve and buying bids of energy and guarantees of origin. Negative values are selling bids of energy and guarantees of origin. Secondary reserve is divided into 2/3 upward and 1/3 downward.

Table 1 – Day-ahead daily bids. Positive values are buying quantities. Negative values are selling quantities.

	NF strategy	NS strategy
Natural gas (MWh)	91.3	95.9
Green hydrogen (MWh)	2.8	1.8
Water (L)	5 133	4 506
Oxygen (kg)	1 357	1 191
CO_2 (t CO_2)	15.1	16.0

7.1.2. Real-time results

In this subsection, we discuss the imbalance and network-related results produced by the combination of two day-ahead strategies (NF and NS) with two real-time strategies (NF and NS).

7.1.2.1. Imbalance results

Imbalances are deviations between day-ahead commitments and real-time realizations. These imbalances represent an extra cost for the aggregator, which tries to minimize it in real-time. In this subsection, we discuss the imbalances produced by the combined day-ahead and real-time strategies mentioned previously: NF-NF; NS-NF; NF-NS; and NS-NS.

Figure 8, Figure 9, and Table 2 show that the NF-NF strategy produced hourly imbalances of guarantees of origin, and daily imbalances of natural gas, green hydrogen, water, oxygen, and CO_2. If we compare these results to those of the other 3 strategies, we can observe that the NF-NF strategy produces the total lowest daily imbalances (i.e., the sum of all electricity, natural gas, green hydrogen, water, oxygen, and CO2 imbalances). However, these imbalances are network-free, meaning that they can be network-infeasible, as it will be shown in the next subsection. These network violations may eventually lead to the unpredictable disconnection of DMERs and prosumers from the networks, which makes it very difficult to estimate the expected network-secure imbalances in this case.

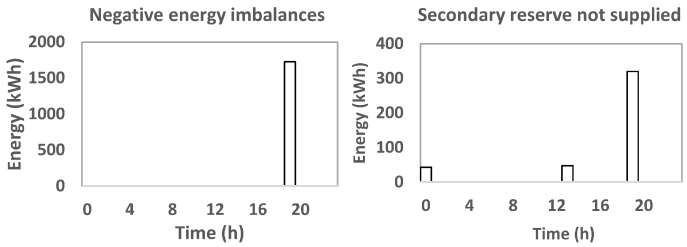

Figure 8 – Negative energy imbalances and secondary reserve not supplied for the NF-NS strategy.

Table 2 – Daily imbalances. Positive and negative values are positive and negative imbalances.

	NF-NF strategy	NF-NS strategy	NS-NF strategy	NS-NS strategy
Natural gas (MWh)	15.7	24.2	19.0	16.7
Green hydrogen (MWh)	0.4	-0.8	0.7	-0.4
Water (L)	-0.5	-0.2	-0.7	-0.9
Oxygen (kg)	-0.1	0.0	-0.2	-0.2
CO_2 (tCO_2)	3.1	4.8	3.8	3.3

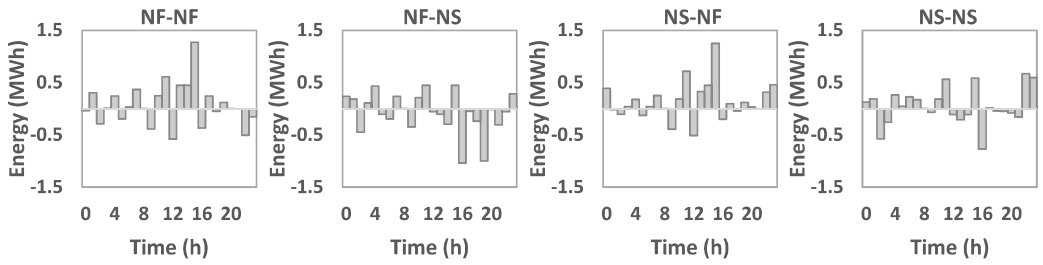

Figure 9 - Guarantees of origin imbalances. Positive and negative values are positive[7] and negative[8] imbalances.

Similar to NF-NF, the NS-NF strategy also produced hourly imbalances of guarantees of origin, and daily imbalances of natural gas, green hydrogen, water, oxygen, and CO_2. This strategy presents the highest daily imbalances, as illustrated in Table 2. As it is network-free in real-time, it allows the aggregator's assets to be scheduled in a way that leads to the violation of technical limits in one or more of the networks considered. However, this option may produce imbalances that create network problems, as discussed previously.

The NF-NS strategy produced the highest daily imbalances of natural gas, green hydrogen, water, oxygen, and CO_2. In addition, it was the only strategy to produce imbalances of electrical energy and secondary reserve, as illustrated in Figure 8. This happens because the aggregator computes bids without considering multi-energy network constraints, and delivers them considering multi-energy network constraints. The imposition of multi-energy network constraints in the real-time stage makes it impossible to deliver all the network-free bids computed in the day-ahead.

Finally, the NS-NS strategy produced lower daily and hourly imbalances than NF-NS and NS-NF strategies. These imbalance results demonstrate that considering multi-energy network constraints in day-ahead and real-time stages reduces imbalances, and at the same time ensures multi-energy network security.

7.1.2.2. Multi-energy network results

Figure 10 illustrates the network problems caused by the four strategies when the three delivery scenarios $s \in \{E, U, D\}$ are simulated across the electricity, gas, and heat networks. The electricity problems are related to voltage violations and are illustrated in the upper-left corner of the figure. The gas network problems are related to WI and HHV violations and are illustrated in the upper-right and lower-left corners. The heat network problems are related to mass flow violations and are illustrated in the lower-right corner.

The results of Figure 10 show that NF-NF and NS-NF strategies caused multiple problems in the electricity, gas, and heat networks. The NF-NF strategy caused 67 voltage, 28 HHV, 1 WI, and 10 mass flow violations, totalizing 106 technical problems. The NS-NF strategy caused 44 voltage, 19 HHV, 2 WI, and 13 mass flow violations, resulting in a total of 78 violations. If we compare the two strategies, we can observe that NF-NF caused 28 more problems than NS-NF. Concerning the severity of the technical problems, we can observe that the NF-NF strategy caused more severe violations when compared to the NS-NF strategy, namely in the heat

[7] A positive imbalance represents an excess buying position or a shortage selling position of the aggregator in real-time compared to the day-ahead.

[8] A negative imbalance represents a shortage buying position or an excess selling position of the aggregator in real-time compared to the day-ahead.

network. It can be concluded that integrating multi-energy network constraints in the day-ahead stage reduces the number and severity of the technical problems, but it does not ensure security in real-time if network constraints are not considered in this stage.

On the contrary, NF-NS and NS-NS strategies did not cause any problems in the electricity, gas, and heat networks, confirming that the consideration of networks' constraints in real-time ensures the reliable delivery of market services.

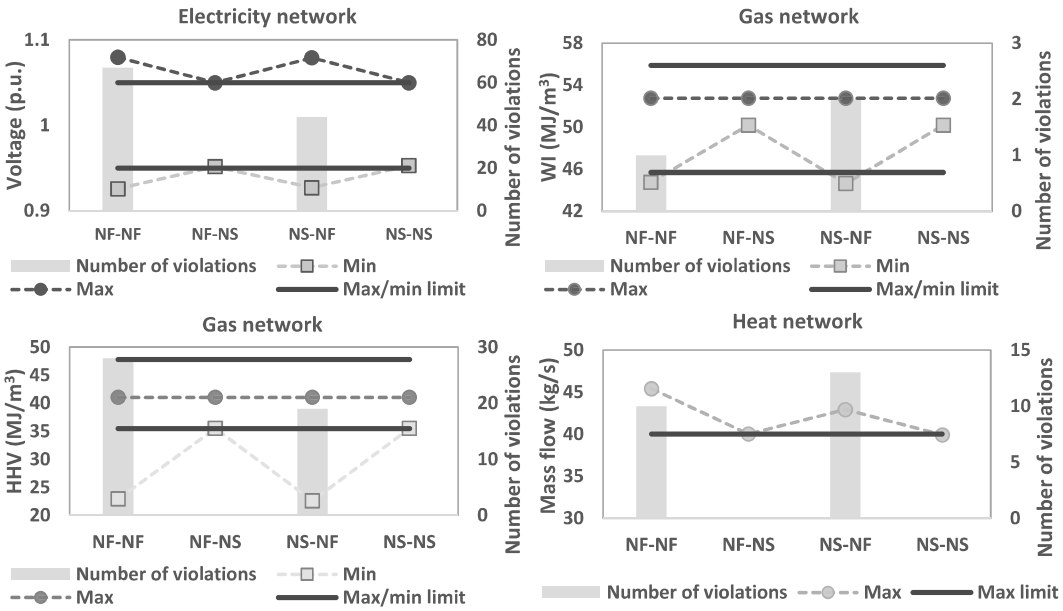

Figure 10 – Multi-energy network problems caused by the four strategies.

7.1.2.3. Computational results

The real-time strategies use a hierarchical MPC with two levels. Both levels were implemented in Python. The optimization subproblems of the aggregator and DSOs in the first level were implemented in Pyomo and solved by the IBM CPLEX v12.9.0 and IPOPT v3.11.1 optimizers, respectively. The aggregator subproblem is a mixed-integer quadratic program, while the DSOs subproblems are non-linear. The experiments were run on a computer with 8 GB RAM and an Intel® Core™ i5.8265U CPU @ clocked at 1.6GHz.

The optimization subproblems in the first level of the hierarchical MPC are solved every hour. Table 3 reports the computational times of these subproblems. As expected, the results show that NF is the fastest approach with a total computational time of 0.96s, followed by the NS with an average total computational time of 11.03min ((3.38 + max(0.05, 0.11, 0.34))*178 ADMM iterations). We used the average values to compute the total computational time since the maximum value is an outlier, i.e., it was only observed once. In addition, we assumed that the aggregator and DSOs subproblems can be solved in parallel.

Both NS and NF approaches ran under the 1-hour requirement, meaning that can be used in the Iberian market setting. In addition, we were able to solve the non-linear DSOs subproblems very efficiently using IPOPT, always ensuring convergence at fast execution times, as illustrated in Table 3.

The controller in the second level of the hierarchical MPC is run every 20s. The execution time of the controller is in the order of milliseconds, far below 20s.

Table 3 - Size and execution time (average, minimum and maximum) of the optimization subproblems in the first level of the hierarchical MPC frameworks.

	Subproblems	Nº of variables	Nº of constraints	MIN time (s)	AVG time (s)	MAX time (s)
NF	**Aggregator**	61 702	84 077	0.36	0.96	1.44
NS	**Aggregator**	64 753	88 106	2.48	3.38	4.56
	Electricity DSO	226	427	0.03	0.05	0.06
	Gas DSO	515	1 023	0.06	0.11	0.29
	Heat DSO	463	1 341	0.08	0.34	0.50

The optimization subproblems of the NS strategy were solved using the ADMM, which has recently been proven to converge for convex problems [25], but also for many non-convex problems [7][10][18] like this one. The absolute tolerance ϵ^{Abs} was set to 0.0001 corresponding to a stop criterion of 0.007 kW in the case of the primal residual.

In the literature, we can find three different types of optimization frameworks for aggregators: distributed (i.e., ADMM frameworks), centralized and decentralized. The distributed framework based on the ADMM, used in this paper, presents pros and cons when compared with the centralized and decentralized frameworks. The next points provide a summary of the comparison regarding four main aspects:

1. Computational complexity: distributed and decentralized frameworks are able to decompose complex problems into smaller and simpler problems and solve them efficiently without linear simplifications. This is an advantage compared to centralized approaches, which rely on linear or other simplifications to solve the problem. This in turn may result in the reduction of the feasible space, or even in the expansion of the space to infeasible areas. For example, centralized approaches usually use simplified electricity, gas, and heat network models (i.e., convex models) to make the joint aggregator and network problem solvable. Nonetheless, these simplifications may generate infeasible physical solutions, like in electricity network models in scenarios of low voltage [36];
2. Privacy: distributed and decentralized frameworks preserve the data privacy of the aggregator and DSOs. On the other hand, in centralized frameworks, aggregators need to have access to network data as they solve the bidding and network problems together;
3. Optimality: the distributed framework enables iterative negotiations between the aggregator and DSO until they arrive at a consensual solution. Decentralized frameworks obtain solutions in 1 or 2 iterations. The reduction of the number of iterations decreases computational complexity, although at a potential high cost since it is very likely that it only reaches sub-optimal solutions. The centralized framework relies on linear or convex simplifications. Therefore, the optimal solution of these simplifications may not be optimal or even feasible in the original space, as previously explained;
4. Communications: the communication requirements are proportional to the number of iterations. Therefore, the distributed framework requires more communications between the different participants than a decentralized framework. On the other hand, centralized frameworks do not require any communications as they solve the problem on their own.

After weighing the three options, the authors decided to use a distributed approach essentially due to the guarantee of reaching a consensual solution in the end for aggregators and DSOs.

7.1.3. Day-ahead and real-time settlement results

Table 4 presents the day-ahead, real-time, and settlement net-costs. The settlement net-costs result from the sum of the day-ahead and real-time net-costs. The formula used to calculate the settlement net-costs is described in Appendix C.

The results of Table 4 show that the NF-NF strategy presents the lowest settlement net-cost of 798€ followed by NS-NF, NS-NS, and NF-NS, with net-cost of 821€, 1033€, and 2759€, respectively. The NF-NF strategy presents the lowest settlement net-cost since it does not consider the multi-energy network constraints in the day-ahead and real-time optimization phases. However, it does not ensure that bids and services delivery are physically feasible, as discussed before. Therefore, this settlement net-cost is theoretical since the aggregator will not be able to deliver the market services negotiated. Even so, it provides an indication of how much the technical limits of the networks are constraining the profits of the aggregator.

The NS-NF strategy presents the second lowest settlement net-cost. Similarly to NF-NF, it also does not ensure network security in real-time, meaning that the delivery of the market services may not be accomplished. As the eventual violation of networks' limits may lead to unpredictable disconnection of DMERs and prosumers, it is impossible to estimate the real network-secure settlement costs of NS-NF and NF-NF. Therefore, these costs are theoretical and can only be used for comparison purposes.

Under real-time network-secure conditions, the NS-NS strategy presents the lowest settlement net-cost. This shows that considering multi-energy network constraints in the day-ahead and real-time problems significantly reduces the real-time net-costs of the aggregator, and consequently its settlement net-costs, while the security of the networks is preserved.

Table 4 - Settlement net-costs. Positive values are costs, and negative values are revenues.

	Net-cost (€)	NF-NF strategy	NF-NS strategy	NS-NF strategy	NS-NS strategy
DA	**Electricity - Energy**	40	40	- 104	- 104
DA	**Electricity - Band**	- 279	- 279	- 260	-260
DA	**Gas**	1 278	1 278	1 342	1 342
DA	**Hydrogen**	-212	-212	-134	-134
DA	**Water**	19	19	17	17
DA	**Oxygen**	-0.2	-0.2	-0.2	-0.2
DA	**Guarantees of origin**	-3	-4	-3	-4
DA	**CO_2**	304	304	317	317
RT	**Reserve activation**	-579	-476	-478	-478
RT	**Energy imbalance**	0	97	0	0
RT	**Reserve not supplied**	0	1 484	0	0
RT	**Gas imbalance**	209	323	126	222
RT	**Hydrogen imbalance**	-58	60	-49	31
RT	**Water imbalance**	-2	-1	-3	-3
RT	**Oxygen imbalance**	0.02	0.01	0.03	0.04
RT	**Guarantees of origin imbalance**	-1	0.9	-1.9	-0.7
RT	**CO_2 imbalance**	78	121	47	83
DA + RT	**Settlement**	798	2 759	821	1 033

7.2. Impacts of the aggregator adopting a green hydrogen policy

In this subsection, we analyze the impacts of the multi-energy aggregator adopting a green hydrogen policy under different prices of green hydrogen and CO_2. This analysis covers several aspects, such as the impacts of different prices on the aggregator's economic performance, green hydrogen production, natural gas consumption, CO_2 emissions, and availability of secondary reserve.

Figure 11 shows that the aggregator cost increases with the increase in CO_2 prices, and decreases with the increase of green hydrogen prices. However, the impact of CO_2 prices is significant, while the impact of green hydrogen prices is very small. In sum, the increase in CO_2 prices will increase the economic pressure on aggregators with natural gas resources like CHPs, incentivizing them to replace these technologies with other electricity-powered technologies, like heat pumps.

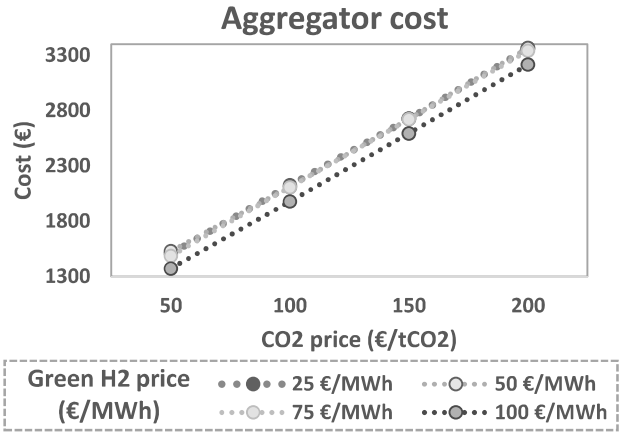

Figure 11 – Impacts of CO_2 and green hydrogen prices on the cost of the aggregator.

The prices of CO_2 emissions and green hydrogen also impact the production of green hydrogen, natural gas consumption, and CO_2 emissions of the DEMRs managed by the aggregator, as illustrated in Figure 12. The production of green hydrogen increases with the increase of their prices, namely when they increase from 75 €/MWh to 100 €/MWh. At this point, the injection of green hydrogen into the gas network becomes very attractive. On the other hand, the prices of CO_2 emissions do not impact the production of green hydrogen as much. This shows that injecting green hydrogen into the gas network is only attractive when green hydrogen prices are higher.

The consumption of natural gas decreases with the increase of CO_2 prices and green hydrogen, as illustrated in Figure 12. In more detail, the increase in CO_2 prices decreases the consumption of natural gas by CHPs, which consume gas to produce heat and carbon-taxed electricity. This is more noticeable when the CO_2 prices increase from 50 €/tCO_2 to 100 €/tCO_2. From 100 €/tCO_2 to 200 €/tCO_2, the room to reduce the consumption of natural gas by CHPs is small. On the other hand, the increase in green hydrogen prices increases the injection of green hydrogen into the gas network and consequently reduces the need to consume natural gas.

The CO_2 emissions produced by the consumption of natural gas follow the same trend as natural gas consumption. This shows that a market with high prices of CO_2 allowances and green hydrogen can contribute to significantly reducing the consumption of natural gas and emitted CO_2.

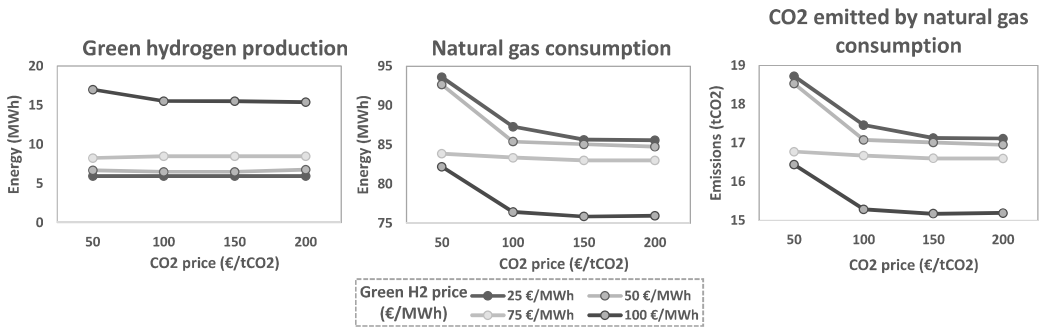

Figure 12 – Impacts of CO_2 and green hydrogen prices on hydrogen production, natural gas consumption, and CO_2 emissions.

The last point to analyze in this subsection is the impact of CO_2 and green hydrogen prices in the provision of secondary reserve for the power system operation. Figure 13 shows that the provision of secondary reserve by the aggregator increases with the increase of green hydrogen prices and the reduction of CO_2 prices. As mentioned before, high CO_2 prices influence the operation of CHPs and consequently reduce the availability of these resources to provide energy and also secondary reserve services. On the other hand, high green hydrogen prices make hydrogen technologies attractive to provide energy and secondary reserve services. In sum, high CO_2 prices discourage the utilization of technologies powered by natural gas to provide secondary reserve. On the other hand, high green hydrogen prices may attract other technologies to provide this essential power system service.

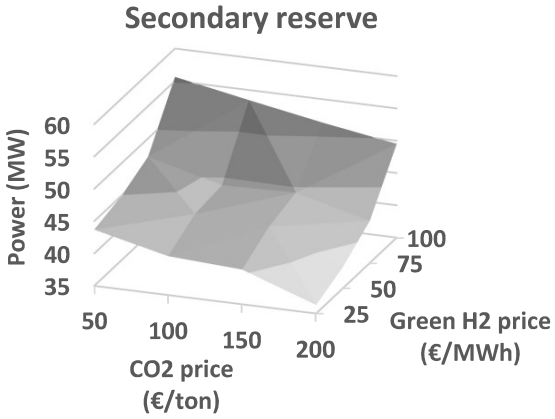

Figure 13 - Impacts of CO_2 and green hydrogen prices in the provision of secondary reserve.

8. Conclusions

This paper presents a new hierarchical MPC framework to assist multi-energy aggregators in the network-secure and real-time delivery of multi-energy services traded in day-ahead electricity, gas, green hydrogen, and carbon markets. The MPC framework uses the ADMM on a rolling horizon to negotiate the network-secure delivery of multi-energy services between aggregators and multi-energy distribution system operators. The multi-energy services include electricity (energy and reserve), natural gas, green hydrogen, and carbon allowances, which result from the real-time optimization of the multi-energy systems managed by aggregators.

We used the proposed hierarchical MPC framework to conduct a series of experiments and studies. The first study discusses and compares the combined performance of day-ahead and

real-time strategies with different levels of multi-energy network observability. The results of this study allow drawing the following conclusions:

1. Network security is only ensured when the constraints of the multi-energy networks are considered in the real-time optimization problem (i.e., in the hierarchical MPC). This means that considering the network constraints only in the day-ahead bidding problem does not guarantee network security;
2. Considering multi-energy network constraints at both day-ahead and real-time optimization stages produces the most cost-effective and reliable solution to aggregators since it minimizes settlement net-costs while ensuring multi-energy network security.

The second study investigates the impacts of multi-energy aggregators adopting a green hydrogen policy under different price scenarios of green hydrogen and carbon prices. Four main conclusions can be derived from the results of this study:

1. Carbon prices can significantly impact the economic performance of multi-energy aggregators with CHPs. High prices may force aggregators to replace CHPs with electricity-powered technologies, like heat pumps;
2. Green hydrogen prices can significantly impact the production of hydrogen, namely its injection into the gas network. The results show that the injection of green hydrogen is only attractive at competitive prices;
3. Green hydrogen and carbon prices can significantly impact the provision of frequency reserve services supplied by DMERs. High green hydrogen prices increase the availability of hydrogen technologies, while high carbon prices reduce the availability of natural gas technologies to provide frequency reserve services;
4. Green hydrogen and carbon prices can significantly impact the consumption of natural gas and its respective CO_2 emissions. High prices of green hydrogen and carbon incentivize the injection of green hydrogen into the gas network and the reduction of natural gas consumption. These two factors together can contribute to significantly reducing natural gas consumption and CO_2 emissions.

Future work consists of investigating the impact of uncertainty in the economic, network, and computational performances of day-ahead and real-time optimization frameworks. Moreover, it is expected the demonstration of the proposed approach in a real-world setting, under the scope of the ATTEST project.

Acknowledgments

The research leading to this work has been carried out as part of the ATTEST project. The ATTEST project was funded by the European Union's Horizon 2020 research and innovation programme under grant agreement No 864298. In addition to the support of the ATTEST project, the work of António Coelho was financed by FCT—Fundação para a Ciência e a Tecnologia (Portuguese Foundation for Science and Technology) through the grant PD/BD/142811/2018.

Appendix A. Distributed multi-energy resource equations

This appendix describes the models of the distributed multi-energy resources not detailed in the main body of the paper. More specifically, it describes the constraints of heat pumps, district heating flexible loads, PVs, battery energy storage systems, and district heating CHPs.

A.1. Heat pump constraints

Constraints (A. 1)-(A. 10) define the operation of the heat pumps. Constraints (A. 1)-(A. 3) define the power limits to consume electricity (A. 1), and provide upward (A. 2) and downward (A. 3) secondary reserve bands. Constraints (A. 5)-(A. 7) define the temperature of the building/room in each delivery scenario (energy (48), upward (52) and downward (53) secondary reserve band). The remaining constraints (A. 8)-(A. 10) impose the comfort range of buildings' occupants.

$$\underline{P_{j,t}^{HP}} \leq P_{j,t}^{HP} \leq \overline{P_{j,t}^{HP}}, \ \forall\ j \in J, \ t \in T \quad \text{(A. 1)}$$

$$U_{j,t}^{HP} \leq P_{j,t}^{HP} - \underline{P_{j,t}^{HP}}, \ \forall\ j \in J, \ t \in T \quad \text{(A. 2)}$$

$$D_{j,t}^{HP} \leq \overline{P_{j,t}^{HP}} - P_{j,t}^{HP}, \ \forall\ j \in J, \ t \in T \quad \text{(A. 3)}$$

$$D_{j,t}^{HP}, U_{j,t}^{HP} \geq 0, \ \forall\ j \in J, \ t \in T \quad \text{(A. 4)}$$

$$\theta_{j,t+1}^{E} = \beta_j \theta_{j,t}^{E} + \left(1-\beta_j\right)\left[\theta_{j,t}^{O} + R_j\left(\eta_j^{HP} P_{j,t}^{HP}\right)\right] + \vartheta_{j,t}, \ \forall\ j \in J, \ t \in T \quad \text{(A. 5)}$$

$$\theta_{j,t+1}^{U} = \beta_j \theta_{j,t}^{U} + \left(1-\beta_j\right)\left[\theta_{j,t}^{O} + R_j\left(\eta_j^{HP} P_{j,t}^{HP} - \eta_j^{HP} U_{j,t}^{HP}\right)\right] + \vartheta_{j,t}, \forall\ j \in J, \ t \in T \quad \text{(A. 6)}$$

$$\theta_{j,t+1}^{D} = \beta_j \theta_{j,t}^{D} + \left(1-\beta_j\right)\left[\theta_{j,t}^{O} + R_j\left(\eta_j^{HP} P_{j,t}^{HP} + \eta_j^{HP} D_{j,t}^{HP}\right)\right] + \vartheta_{j,t}, \ \forall\ j \in J, \ t \in T \quad \text{(A. 7)}$$

$$\underline{\theta_j} \leq \theta_{j,t+1}^{E} \leq \overline{\theta_j}, \quad \forall\ j \in J, \ t \in T \quad \text{(A. 8)}$$

$$\underline{\theta_j} \leq \theta_{j,t+1}^{U} \leq \overline{\theta_j}, \quad \forall\ j \in J, \ t \in T \quad \text{(A. 9)}$$

$$\underline{\theta_j} \leq \theta_{j,t+1}^{D} \leq \overline{\theta_j}, \quad \forall\ j \in J, \ t \in T \quad \text{(A. 10)}$$

A.2. District heating flexible load constraints

Constraints (A. 1)-(A. 10) are also used to model the operation of district heating flexible loads. However, instead of using electric power variables $\left\{P_{j,t}^{HP}, D_{j,t}^{HP}, U_{j,t}^{HP}\right\}$, in this case we use thermal variables $\left\{P_{j,t}^{DH}, D_{j,t}^{DH}, U_{j,t}^{DH}\right\}$ without considering the coefficients of performance.

A.3. Photovoltaic system constraints

Constraints (A. 11)-(A. 13) define the operation of PVs. Constraint (A. 11) defines the power generated by the system, while constraints (A. 12) and (A. 13) define the secondary reserve bands provided by PV systems.

$$0 \leq P_{j,t}^{PV} \leq \overline{P_j^{PV}}, \ \forall\ \ j \in J, \ t \in T \quad \text{(A. 11)}$$

$$0 \leq U_{j,t}^{PV} \leq \overline{P_j^{PV}} - P_{j,t}^{PV}, \forall\ \ j \in J, \ t \in T \quad \text{(A. 12)}$$

$$0 \leq D_{j,t}^{PV} \leq P_{j,t}^{PV}, \ \forall\ \ j \in J, \ t \in T \quad \text{(A. 13)}$$

A.4. Battery energy storage systems

Constraints (A. 14)-(A. 23) define the operation of the battery energy storage systems. Constraints (A. 14) and (A. 15) define the limits of charging and discharging. Constraints (A. 16) and (A. 17) define the state-of-charge and the limits of the storage system.

$$0 \leq P_{j,t}^{Sto,-} \leq \left(1 - b_{j,t}^{Sto,E}\right)\overline{P_J^{Sto,-}}, \ \forall\, j \in J, \ t \in T \quad \text{(A. 14)}$$

$$0 \leq P_{j,t}^{Sto,+} \leq b_{j,t}^{Sto,E}\overline{P_J^{Sto,+}}, \ \forall\, j \in J, \ t \in T \quad \text{(A. 15)}$$

$$SOC_{j,t+1}^{Sto,E} = SOC_{j,t}^{Sto,E} + \left(P_{j,t}^{Sto,+}\eta_j - \frac{P_{j,t}^{Sto,-}}{\eta_j}\right)\Delta t,\ \forall j \in J,\ \ t \in T \quad \text{(A. 16)}$$

$$\underline{SOC_j^{Sto,E}} \leq SOC_{j,t+1}^{Sto,E} \leq \overline{SOC_j^{Sto,E}},\ \forall j \in J,\ \ t \in T \quad \text{(A. 17)}$$

Constraints (A. 18)-(A. 23) define the secondary reserve provided by the battery energy storage system. Constraints (A. 18)-(A. 21) define the power limits, while constraints (A. 22) and (A. 23) define the energy limits.

$$\boldsymbol{0 \leq U_{j,t}^{Sto,-} \leq \overline{P_j^{Sto,-}} - P_{j,t}^{Sto,-},\ \forall j \in J,\ \ t \in T} \quad \text{(A. 18)}$$

$$\boldsymbol{0 \leq U_{j,t}^{Sto,+} \leq P_{j,t}^{Sto,+},\ \forall j \in J,\ \ t \in T} \quad \text{(A. 19)}$$

$$\boldsymbol{0 \leq D_{j,t}^{Sto,+} \leq \overline{P_j^{Sto,+}} - P_{j,t}^{Sto,+},\ \forall j \in J,\ \ t \in T} \quad \text{(A. 20)}$$

$$\boldsymbol{0 \leq D_{j,t}^{Sto,-} \leq P_{j,t}^{Sto,-},\ \forall j \in J,\ \ t \in T} \quad \text{(A. 21)}$$

$$\boldsymbol{\left(\frac{U_{j,t}^{Sto,-}}{\eta_j} + U_{j,t}^{Sto,+}\eta_j\right)\Delta t \leq SOC_{j,t+1}^{Sto,E} - \underline{SOC_j^{Sto,E}},\ \forall j \in J,\ \ t \in T} \quad \text{(A. 22)}$$

$$\boldsymbol{\left(\frac{D_{j,t}^{Sto,-}}{\eta_j} + D_{j,t}^{Sto,+}\eta_j\right)\Delta t \leq \overline{SOC_j^{Sto,E}} - SOC_{j,t+1}^{Sto,E},\ \forall j \in J,\ \ t \in T} \quad \text{(A. 23)}$$

A.5. Combined heat and power constraints

Constraints (A. 24)-(A. 33) define the operation of the CHPs. Constraints (A. 24)-(A. 33) define the gas consumption limits (A. 24), electricity (A. 25) and heat (A. 26) generated by them. Constraints (A. 27)-(A. 32) define the secondary reserve bands provided by the CHPs in both upward and downward directions.

$$\underline{P_{j,t}^{CHP,G}} \leq P_{j,t}^{CHP,G} \leq \overline{P_{j,t}^{CHP,G}},\ \forall\ j \in J,\ \ t \in T \quad \text{(A. 24)}$$

$$P_{j,t}^{CHP,E} = \eta_j^{CHP,E} P_{j,t}^{CHP,G},\qquad \forall\ j \in J, t \in T \quad \text{(A. 25)}$$

$$P_{j,t}^{CHP,H} = \eta_j^{CHP,H} P_{j,t}^{CHP,G},\qquad \forall j \in J, t \in T \quad \text{(A. 26)}$$

$$0 \leq U_{j,t}^{CHP,G} \leq \overline{P_{j,t}^{CHP,G}} - P_{j,t}^{CHP,G},\quad \forall\ j \in J,\ \ t \in T \quad \text{(A. 27)}$$

$$U_{j,t}^{CHP,E} = \eta_j^{CHP,E}.\, U_{j,t}^{CHP,G},\quad \forall\ j \in J,\ \ t \in T \quad \text{(A. 28)}$$

$$U_{j,t}^{CHP,H} = \eta_j^{CHP,H}.\, U_{j,t}^{CHP,G},\quad \forall\ j \in J,\ \ t \in T \quad \text{(A. 29)}$$

$$0 \leq D_{j,t}^{CHP,G} \leq P_{j,t}^{CHP,G} - \underline{P_{j,t}^{CHP,G}},\quad \forall\ j \in J,\ \ t \in T \quad \text{(A. 30)}$$

$$D_{j,t}^{CHP,E} = \eta_j^{CHP,E}.\, D_{j,t}^{CHP,G},\quad \forall\ j \in J,\ \ t \in T \quad \text{(A. 31)}$$

$$D_{j,t}^{CHP,H} = \eta_j^{CHP,H}.\, D_{j,t}^{CHP,G},\quad \forall\ j \in J,\ \ t \in T \quad \text{(A. 32)}$$

CHPs are only capable of providing 100% of their power within 60 s [37] making them slower than other resources to respond to set-points. Constraint (A. 33) limits the response of the CHPs to a fraction of its maximum power. This makes the CHPs capable of complying with the AGC signal.

$$U_{j,t}^{CHP,G}, D_{j,t}^{CHP,G} \leq \mu^{CHP}.\, \overline{P_{j,t}^{CHP,G}},\quad \forall\ j \in J,\ \ t \in T \quad \text{(A. 33)}$$

Appendix B. DSO subproblems: electricity and heat flow optimization models

This appendix describes the electricity and heat flow optimization models not detailed in the main body of the paper.

B.1. Electricity flow optimization model

The electricity flow optimization problem (B. 1)-(B. 7) is used by the electricity DSO to make network-secure the electricity delivery scenarios computed by the aggregator.

B.1.1. Objective function

The objective function (B. 1) minimizes the augmented Lagrangian penalty, which penalizes the calculation of network-secure electricity delivery scenarios that deviate from the aggregator's preferences.

$$Min \sum_{n \in N^E} \left[\pi_n^E \left(P_n^E - \hat{P}_n^E \right) + \frac{\rho}{2} \left(P_n^E - \hat{P}_n^E \right)^2 \right] \quad \text{(B. 1)}$$

B.1.2. Network constraints

The electricity network is modelled using the non-convex formulation of the branch flow model [38][39]. Constraints (B. 2)-(B. 5) are the branch power flow equations. Constraints (B. 6) and (B. 7) set the limits of the square of the voltage and current magnitudes.

$$P_{m,n}^F = \frac{\hat{P}_n^E}{SB} + \sum_{i:n \to i} P_{n,i}^F + r_{m,n} \ell_{m,n}, \quad \forall (m,n) \in B^E \quad \text{(B. 2)}$$

$$Q_{m,n}^F = Q_n^E + \sum_{i:n \to i} Q_{n,i}^F + x_{m,n} \ell_{m,n}, \quad \forall (m,n) \in B^E \quad \text{(B. 3)}$$

$$v_n = v_m - 2\left(r_{m,n} P_{m,n}^F + x_{m,n} Q_{m,n}^F \right) + \left(r_{m,n}^2 + x_{m,n}^2 \right) \ell_{m,n}, \quad \forall (m,n) \in B^E \quad \text{(B. 4)}$$

$$\ell_{m,n} v_m = {P_{m,n}^F}^2 + {Q_{m,n}^F}^2, \quad \forall (m,n) \in B^E \quad \text{(B. 5)}$$

$$\underline{v_n} \leq v_n \leq \overline{v_n}, \quad \forall n \in N^E \quad \text{(B. 6)}$$

$$0 \leq \ell_{m,n} \leq \overline{\ell_{m,n}}, \quad \forall (m,n) \in B^E \quad \text{(B. 7)}$$

B.2. Heat flow optimization model

The heat flow optimization problem (B. 8)-(B. 19) is used by the heat DSO to make network-secure the heat delivery scenarios computed by the aggregator.

B.2.1. Objective function

The objective function (B. 8) minimizes the augmented Lagrangian penalty, which penalizes the calculation of network-secure heat delivery scenarios that deviate from the aggregator's preferences.

$$Min \sum_{i \in N^H} \left[\pi_i^H \left(P_i^H - \hat{P}_i^H \right) + \frac{\rho}{2} \left(P_i^H - \hat{P}_i^H \right)^2 \right] \quad \text{(B. 8)}$$

B.2.2. Network constraints

The heat network consists of identical supply and return networks. Hydraulic and thermal optimizations are performed to calculate the mass flows and temperatures of pipes and nodes.

In this model, the temperature of generator supply nodes and load return nodes are predefined, as well as the heat power at all nodes, except the slack node.

B.2.2.1. Hydraulic model

Constraints (B. 9) and (B. 10) define the conservation of mass and pressure drop, respectively. Constraint (B. 11) defines the pressure limits. Constraints (B. 11) and (87) set the mass flow limits of pipes and loads/generators, respectively [40]. To relax the problem, the heat direction flow was initialized for each hour based on the algorithm presented in [41] and remained static for the rest of the iterations.

$$\sum_{j:j\to i} m_{j,i}^{a} - \sum_{j:i\to j} m_{i,j}^{a} = A_i^a mq_i, \ \ \forall\, a \in \{S,R\}, \ i \in N^H \tag{B. 9}$$

$$p_i^{H,a} - p_j^{H,a} = k_{i,j}^{a} m_{i,j}^{a} \left| m_{i,j}^{a} \right|, \ \ \forall\, a \in \{S,R\}, \ \ (i,j) \in B^H \tag{B. 10}$$

$$\underline{p_i^{H,a}} \le p_i^{H,a} \le \overline{p_i^{H,a}}, \ \ \forall\, a \in \{S,R\}, \ \ i \in N^H \tag{B. 11}$$

$$\underline{m_{i,j}^{a}} \le m_{i,j}^{a} \le \overline{m_{i,j}^{a}}, \ \ \forall\, a \in \{S,R\}, \ \ (i,j) \in B^H \tag{B. 12}$$

$$\underline{mq_i} \le mq_i \le \overline{mq_i}, \ \ \forall\, i \in N^H \tag{B. 13}$$

B.2.2.2. Thermal model

The thermal model (B. 14)-(B. 19) is used to determine the temperatures at each network node. Constraint (B. 14) is the heat power equation of the loads and generators. The temperature drop constraint (B. 15) defines the temperature at the end node of the pipe. Constraints (B. 16) and (B. 17) set the limits of the temperatures at the end and start nodes of the pipe. Constraint (B. 18) defines the conservation of energy. Constraint (B. 19) connects equation (B. 14) to the remaining constraints of the thermal model by imposing that the temperatures of mass flowing through the node are equal to the temperatures mixed at the node.

$$\hat{P}_i^H = CP \cdot mq_i(\theta_i^S - \theta_i^R), \ \ \forall\, i \in N^H \tag{B. 14}$$

$$\theta_{i,j}^{End,a} = (\theta_{i,j}^{Start,a} - \theta^{Amb}) e^{\frac{h.L}{CP \cdot m_{i,j}^{a}}} + \theta^{Amb}, \ \ \forall\, a \in \{S,R\}, \ \ (i,j) \in B^H \tag{B. 15}$$

$$\underline{\theta_{i,j}^{End,a}} \le \theta_{i,j}^{End,a} \le \overline{\theta_{i,j}^{End,a}}, \ \ \forall\, a \in \{S,R\}, \ \ (i,j) \in B^H \tag{B. 16}$$

$$\underline{\theta_{i,j}^{Start,a}} \le \theta_{i,j}^{Start,a} \le \overline{\theta_{i,j}^{Start,a}}, \ \ \forall\, a \in \{S,R\}, \ \ (i,j) \in B^H \tag{B. 17}$$

$$\sum_{j:j\to i} \theta_{j,i}^{End,a} m_{j,i}^{a} = \theta_i^a \sum_{j:i\to j} m_{i,j}^{a}, \ \ \forall\, a \in \{S,R\}, \ \forall\, i \in N^H \tag{B. 18}$$

$$\theta_i^a = \theta_{i,j}^{Start,a}, \forall\, a \in \{S,R\}, \ \ (i,j) \in B^H \tag{B. 19}$$

Appendix C. Settlement equation

The equation (C. 1) defines the settlement net-cost of the aggregator. This equation is divided into 7 terms. The first term (C. 2) is the net-cost of buying and selling electricity and secondary reserve at day-ahead and real-time market stages. The remaining terms (C. 3)-(C. 8)are the net-costs of trading natural gas (C. 3), green hydrogen (C. 4), water (C. 5), oxygen (C. 6), guarantees of origin (C. 7), and CO_2allowances (C. 8) at day-ahead and real-time stages.

$$Settlement = \sum_{t\in T} (f_t^E + f_t^{GO}) + f^G + f^{Hy} + f^{H_2 0} + f^{0_2} + f^C \tag{C. 1}$$

$$f_t^E = \lambda_t^E P_t^{E,DA} \Delta t - \lambda_t^B (U_t^{E,DA} + D_t^{E,DA}) + (\lambda_t^{D,RT} D_t^{E,RT} - \lambda_t^{U,RT} U_t^{E,RT}) \Delta t + (\lambda_t^{E,-} \Delta P_t^{E,-} - \lambda_t^{E,+} \Delta P_t^{E,+}) \Delta t + \lambda_t^{B,-} (\Delta U_t^E + \Delta D_t^E) \Delta t \tag{C. 2}$$

$$f^{G} = \lambda^{G,DA} P^{G,DA} \Delta t + \lambda^{G,RT} (\Delta P^{G,-} - \Delta P^{G,+}) \Delta t \quad \text{(C. 3)}$$

$$f^{H_2} = \lambda^{H_2} (-P^{P2G,H_2,DA} + \Delta P^{P2G,H_2,-} - \Delta P^{P2G,H_2,+}) \Delta t \quad \text{(C. 4)}$$

$$f^{H_2O} = \lambda^{H_2O} (P^{P2G,E,DA} + \Delta P^{P2G,E,-} - \Delta P^{P2G,E,+}) c^{H_2O} \Delta t \quad \text{(C. 5)}$$

$$f^{0_2} = \lambda^{0_2} (-P^{P2G,E,DA} + \Delta P^{P2G,E,+} - \Delta P^{P2G,E,-}) c^{O_2} \Delta t \quad \text{(C. 6)}$$

$$f_t^{GO} = \lambda_t^{GO} (P_t^{GO} + \Delta P_t^{GO,-} - \Delta P^{GO,+}) \Delta t \quad \text{(C. 7)}$$

$$f^{C} = \lambda^{CO_2} (P^{C,DA} + \Delta P^{C,-} - \Delta P^{C,+}) c^{CO_2,G} \Delta t \quad \text{(C. 8)}$$

References

[1] European Commission, Communication from the Commission to the European Parliament, the Council, the European Economic and Social Committee and the Committee of the Regions, 2020.

[2] R.J. Bessa, M.A. Matos, Optimization models for EV aggregator participation in a manual reserve market, IEEE Transactions on Power Systems. 28 (2013) 3085–3095. doi:10.1109/TPWRS.2012.2233222.

[3] R.J. Bessa, M.A. Matos, Optimization models for an EV aggregator selling secondary reserve in the electricity market, Electric Power Systems Research. 106 (2014) 36–50. doi:10.1016/j.epsr.2013.08.006.

[4] J. Iria, F. Soares, M. Matos, Optimal bidding strategy for an aggregator of prosumers in energy and secondary reserve markets, Applied Energy. 238 (2019) 1361–1372. doi:10.1016/j.apenergy.2019.01.191.

[5] J.P. Iria, F.J. Soares, M.A. Matos, Trading Small Prosumers Flexibility in the Energy and Tertiary Reserve Markets, IEEE Transactions on Smart Grid. (2018) 1–1. doi:10.1109/TSG.2018.2797001.

[6] J. Iria, F. Soares, M. Matos, Optimal supply and demand bidding strategy for an aggregator of small prosumers, Applied Energy. 213 (2018) 658–669. doi:10.1016/j.apenergy.2017.09.002.

[7] A. Coelho, J. Iria, F. Soares, Network-secure bidding optimization of aggregators of multi-energy systems in electricity, gas, and carbon markets, Applied Energy. 301 (2021) 117460. doi:10.1016/j.apenergy.2021.117460.

[8] N. Neyestani, M. Yazdani-Damavandi, M. Shafie-khah, G. Chicco, J.P.S. Catalao, Stochastic Modeling of Multienergy Carriers Dependencies in Smart Local Networks With Distributed Energy Resources, IEEE Transactions on Smart Grid. 6 (2015) 1748–1762. doi:10.1109/TSG.2015.2423552.

[9] E. Vrettos, F. Oldewurtel, G. Andersson, Robust Energy-Constrained Frequency Reserves from Aggregations of Commercial Buildings, IEEE Transactions on Power Systems. 31 (2016) 4272–4285. doi:10.1109/TPWRS.2015.2511541.

[10] J. Iria, P. Scott, A. Attarha, Network-constrained bidding optimization strategy for aggregators of prosumers, Energy. 207 (2020) 118266. doi:10.1016/j.energy.2020.118266.

[11] H. Wang, S. Riaz, P. Mancarella, Integrated techno-economic modeling, flexibility analysis, and business case assessment of an urban virtual power plant with multi-market co-optimization, Applied Energy. 259 (2020) 114142. doi:10.1016/j.apenergy.2019.114142.

[12] J. Naughton, H. Wang, S. Riaz, M. Cantoni, P. Mancarella, Optimization of multi-energy virtual power plants for providing multiple market and local network services, Electric Power Systems Research. 189 (2020) 106775. doi:10.1016/j.epsr.2020.106775.

[13] K. Steriotis, K. Smpoukis, N. Efthymiopoulos, G. Tsaousoglou, P. Makris, E. (Manos) Varvarigos, Strategic and network-aware bidding policy for electric utilities through the optimal orchestration of a virtual and heterogeneous flexibility assets' portfolio, Electric

Power Systems Research. 184 (2020) 106302. doi:10.1016/j.epsr.2020.106302.
[14] L. Bobo, A. Venzke, S. Chatzivasileiadis, Second-order cone relaxations of the optimal power flow for active distribution grids: Comparison of methods, International Journal of Electrical Power & Energy Systems. 127 (2021) 106625. doi:10.1016/j.ijepes.2020.106625.
[15] J. Iria, F. Soares, Real-time provision of multiple electricity market products by an aggregator of prosumers, Applied Energy. 255 (2019) 113792. doi:10.1016/j.apenergy.2019.113792.
[16] C. Zhang, Q. Wang, J. Wang, M. Korpås, M.E. Khodayar, Strategy-making for a proactive distribution company in the real-time market with demand response, Applied Energy. 181 (2016) 540–548. doi:10.1016/J.APENERGY.2016.08.058.
[17] A. Attarha, P. Scott, S. Thiébaux, Network-aware co-optimisation of residential DER in energy and FCAS markets, Electric Power Systems Research. 189 (2020) 106730. doi:10.1016/j.epsr.2020.106730.
[18] J. Iria, P. Scott, A. Attarha, D. Gordon, E. Franklin, MV-LV network-secure bidding optimisation of an aggregator of prosumers in real-time energy and reserve markets, Energy. 242 (2022) 122962. doi:10.1016/j.energy.2021.122962.
[19] E. SPOT, N. Pool, OMIE, OPCOM, GME, OTE, TGE, EUPHEMIA Public Description - PCR Market Coupling Algorithm, Price Coupling of Regions (PCR), 2016.
[20] A. Pillay, S. Prabhakar Karthikeyan, D.P. Kothari, Congestion management in power systems - A review, International Journal of Electrical Power and Energy Systems. 70 (2015) 83–90. doi:10.1016/j.ijepes.2015.01.022.
[21] Entidade Reguladora dos Serviços Energéticos (ERSE), Manual of procedures for the management of the power system [in Portuguese], 2020.
[22] Entidade Reguladora dos Serviços Energéticos (ERSE), Manual of procedures for the access to natural gas infrastructures [in Portuguese], 2017.
[23] European Commission, Communication from the Commission to the European Parliament, the Council, the European Economic and Social Committee and the Committee of the Regions: A hydrogen strategy for a climate-neutral Europe, Brussels, 2020.
[24] European Commission, Commission Delegated Regulation (EU) 2019/331, 2018.
[25] S. Boyd, N. Parikh, E. Chu, B. Peleato, J. Eckstein, Distributed Optimization and Statistical Learning via the Alternating Direction Method of Multipliers, Foundations and Trends® in Machine Learning. 3 (2010) 1–122. doi:10.1561/2200000016.
[26] M. Abeysekera, J. Wu, N. Jenkins, M. Rees, Steady state analysis of gas networks with distributed injection of alternative gas, Applied Energy. 164 (2016) 991–1002. doi:10.1016/j.apenergy.2015.05.099.
[27] H. de Vries, A. V. Mokhov, H.B. Levinsky, The impact of natural gas/hydrogen mixtures on the performance of end-use equipment: Interchangeability analysis for domestic appliances, Applied Energy. 208 (2017) 1007–1019. doi:10.1016/j.apenergy.2017.09.049.
[28] Carlos M. Correa-Posada, P. Sánchez-Martín, Gas Network Optimization: A comparison of Piecewise Linear Models, Lecture Notes in Computational Vision and Biomechanics. 5 (2012) 133–159. doi:10.1007/978-94-007-4552-0_6.
[29] E.A.M. Cesena, E. Loukarakis, N. Good, P. Mancarella, Integrated Electricity-Heat-Gas Systems: Techno-Economic Modeling, Optimization, and Application to Multienergy Districts, Proceedings of the IEEE. (2020) 1–19. doi:10.1109/jproc.2020.2989382.
[30] C. Fu, J. Lin, Y. Song, J. Li, J. Song, Optimal Operation of an Integrated Energy System Incorporated With HCNG Distribution Networks, IEEE Transactions on Sustainable Energy. 11 (2020) 2141–2151. doi:10.1109/TSTE.2019.2951701.
[31] ENTSO-E, Transparency Platform, (n.d.). https://transparency.entsoe.eu/dashboard/show .

[32] REN, SIMEE - Mercado Diário e Intradiário, (n.d.). https://www.mercado.ren.pt/PT/Electr/InfoMercado/InfOp/MercOmel/Paginas/default.aspx.
[33] MIBGAS, Daily natural gas prices, (n.d.). https://www.mibgas.es/pt/market-results.
[34] ATTEST - Home, (n.d.). https://attest-project.eu/.
[35] ATTEST H2020 | Zenodo, (n.d.). https://zenodo.org/communities/attest-eu/?page=1&size=20.
[36] J. Iria, M. Heleno, G. Cardoso, Optimal sizing and placement of energy storage systems and on-load tap changer transformers in distribution networks, Applied Energy. 250 (2019) 1147–1157. doi:10.1016/j.apenergy.2019.04.120.
[37] W. Energy, Energy Solutions, 2020.
[38] M.E. Baran, F.F. Wu, Optimal sizing of capacitors placed on a radial distribution system, IEEE Transactions on Power Delivery. 4 (1989) 735–743. doi:10.1109/61.19266.
[39] M.E. Baran, F.F. Wu, Optimal capacitor placement on radial distribution systems, IEEE Transactions on Power Delivery. 4 (1989) 725–734. doi:10.1109/61.19265.
[40] X. Liu, J. Wu, N. Jenkins, A. Bagdanavicius, Combined analysis of electricity and heat networks, Applied Energy. 162 (2016) 1238–1250. doi:10.1016/J.APENERGY.2015.01.102.
[41] Y. Cao, W. Wei, L. Wu, S. Mei, M. Shahidehpour, Z. Li, Decentralized Operation of Interdependent Power Distribution Network and District Heating Network: A Market-Driven Approach, IEEE Transactions on Smart Grid. 10 (2018) 5374–5385. doi:10.1109/TSG.2018.2880909.
[42] J. Hu, G. Yang, H.W. Bindner, Y. Xue, Application of Network-Constrained Transactive Control to Electric Vehicle Charging for Secure Grid Operation, IEEE Transactions on Sustainable Energy. 8 (2017) 505–515. doi:10.1109/TSTE.2016.2608840.